Numerical Assessment of the Scale Effects on the Propulsive Performance of a Ship with Gate Rudder System

Md Daluar Hussain [a], Md Mashud Karim [b]*, Noriyuki Sasaki [c]
[a] Department of Naval Architecture and Marine Engineering, Military Institute of Science and Technology (MIST), Bangladesh
[b] Department of Naval Architecture and Marine Engineering, Bangladesh University of Engineering and Technology (BUET), Bangladesh
[c] Department of Naval Architecture, Ocean and Marine Engineering, University of Strathclyde, UK
*Corresponding author's email address: mmkarim@name.buet.ac.bd

Abstract

Several energy-saving methods have been implemented on ships to improve propulsion efficiency, reducing fuel consumption and carbon dioxide emissions. The Gate Rudder System, as a novel energy-saving and maneuvering device, reduces fuel consumption by up to 14 % compared to the conventional flap rudder system, as confirmed by the sea trial test of a container ship with a gate rudder system. The power savings achieved by the ship with the Gate Rudder system exceeded projections based on model tests. With the motivation of evaluating this discrepancy, this research aims to investigate the propulsive performance of a cargo ship with a gate rudder system as well as the scale effects on its performance, considering two different models of 3 m and 6 m in length, as well as a full-scale ship of 69 m in length. RANSE-based CFD analyses with the Shear Stress Transport (SST) k-ω turbulence model were performed to investigate the ship's propulsive performance and power savings at full load and sea trial conditions with both conventional and gate rudder arrangements. For multi-phase flows, the volume of fluid method (VOF) was used to account for free surface effects, and the model was unconstrained by heave and pitch. Grid convergence, verification, and validation studies were carried out to ensure the accuracy of the numerical studies. Improved propulsive performance and more than 12 % power savings for the ship with the gate rudder system have been achieved at both loading conditions compared to the conventional rudder for the selected cargo ship. The study also observes scale effects, which reveal that the gate rudder of the larger model generates more thrust compared to the smaller one.

Keywords: Fuel consumption, novel energy-saving devices, conventional rudder, gate rudder system, propulsive performance, scale effects

1 Introduction

Energy efficiency and greenhouse gas (GHG) emission reduction are now important factors in global shipping. According to the 4th IMO GHG study, the shipping industry shared 2.89% of global GHG emissions in 2018, which has increased from 2.76% in 2012. The emissions of total shipping have increased from 977 million tons in 2012 to 1,076 million tons in 2018, which is a 9.6% increase (IMO, 2020). As a result of increased maritime transportation, as well as challenges in implementing efficient fuel efficiency measures, the contribution to global emissions from shipping is likely to rise. It is projected that shipping emissions will increase from about 90% of 2008 emissions in 2018 to 90–130% of 2008 emissions by 2050 (IMO, 2020). The GHG strategy targets reducing CO2 emissions by 40% by 2030 and 70% by 2050 compared to 2008 (IMO, 2020). Therefore, the design standards for marine propulsion systems are becoming increasingly stringent. Not only must optimum propulsive efficiency be met, but also comfort and environmental standards and regulations set by IMO. Because of the increasingly stringent regulatory environment, minimizing emissions from ships has become a pressing issue. Numerous technological and operational methods have been researched by the marine industry to make the ship energy efficient and hence to attain specified carbon emission standards, e.g., EEDI standards by IMO. To maintain IMO requirements for Energy Efficiency Design Index (EEDI), fuel-efficient ships are suggested to reduce CO2 emissions for both international and domestic shipping (Hasan and Karim, 2020). The reduction of emissions as well as fuel consumption and power savings can be achieved by introducing various methods such as energy-saving devices, LNG-fueled propulsion, renewable energy utilization, improved hull design, use of advanced anti-fouling paint, and optimum weather routing (Mofor et al., 2015; Hussain and Amin, 2021).

The use of unconventional propulsive combinations could be a beneficial approach to meet the requirements of EEDI. Among these solutions were recent advancements in novel energy-saving devices (ESD) applied to the underwater hull and renewable energy-saving devices onboard, as well as alternative fuel sources and sophisticatedly optimized hull forms (De Jong., 2011). The propulsive performance of a ship hull is strongly influenced by the rudder-propeller interaction and the complex flow field of the aft region of a ship is affected by the position of the rudder (Karim and Naz, 2019). The propeller's propulsive performance has a dominant influence on the distribution of the wake field. The interference effect from the rudder changes the distribution of the wake field around the propeller (Turkmen et al., 2016). It is essential to understand the inflow properties of a propeller to design a complementary ESD (De Jong, 2011). Recovery of propeller rotational losses by fins positioned in

front or after a propeller (i.e., pre- or post-swirl devices) and recovery of viscous resistance losses by ducts or fins placed in front of a propeller to generate thrust (i.e., flow improvement or wake equalizing device) are two forms of ESDs (Sasaki et al. 2015). Thus, ESD must be designed considering the flow field, the interaction of the hull and propulsors (Sasaki et al., 2015). There have been several concepts for the arrangement of a rudder and a propeller to improve propulsive efficiency. Energy-saving devices such as pre- and post-swirl stators, propeller boss cap fins, propeller ducts or Mewis ducts combined with contra-rotating and tip-loaded blades have been investigated as reliable methods of improving propulsive efficiency and reducing energy consumption. ducts, pre-swirl stators, pre-nozzles, and other energy-saving devices. However, the main challenges involved with the implementation of these ESDs are limited to the type and form of vessels.

Recently, a new concept for propeller-rudder arrangement has been introduced by Sasaki et al. (2015), named the "Gate Rudder" system, as shown in Fig. 1, which allows improved fuel efficiency and reduced emissions. Sasaki et al. (2018) described the Gate Rudder system as a novel propulsion arrangement that is based on a new notion of elementary propulsive efficiency and optimizes it in a ship's wake to recover more energy (Sasaki et. al, 2018). It is very well known that the ship rudder is one of the main sources of appendage resistance (Sasaki et al., 2018). The innovative rudder system consists of two unique shaped rudder blades that are arranged in parallel on both sides of the propeller rather than behind it, as shown in Fig. 1, reducing rudder resistance, and generating thrust to save fuel consumption (Sasaki et al. 2017). The rudder blades, which work like a duct, produce 5–15% of the additional thrust generated by the propeller, reducing the high propeller loading (Sasaki and Atlar, 2018). In contrast to the additional resistance caused by the conventional rudder, the Gate Rudder System takes advantage of the greater thrust provided by the two rudder blades (Sasaki, 2018). Each blade has its own rudder stock, allowing it to be controlled separately (Sasaki 2018). Unlike the traditional arrangement of the rudder in the propeller slipstream, the gate rudder will serve as a large diameter duct which is about 120%–140% of the propeller diameter, guiding the larger region of favorable stern flow onto the propeller plane (Sasaki et. al, 2018). This large open accelerating duct is a type of energy-saving device that collects the streamlines distorted by the hull surface with viscosity loss in order to recover viscous resistance loss (Sasaki et. al, 2015). The duct effect is used by the Gate Rudder to transform fluid force into thrust (Turkmen et al., 2016). The duct effect occurs when a fluid enters a duct with a particular cross-sectional configuration that encircles a propeller to create a velocity difference, which causes the forward component of the lifting power to contribute to thrust (Turkmen et al., 2016). The configuration significantly improves the noise and vibration signature while providing outstanding maneuverability (Tacar et al. 2020). The high-lift rudder foils are placed on either side of the propeller, allowing for faster turning, course adjustments, and crash stops (Sasaki et al., 2016).

Fig. 1 Installed Gate Rudder System in actual ship (a) MV Shigenobu (b) Shinmon Maru

Gate Rudder has already been used on three different ships; among those, one is a container ship, and the other two are general cargo ships. The system was installed in a 2400 GT container ship for the first time, and full-scale sea trials were successfully completed in November 2017 in Japan (Sasaki et al., 2020). According to the trial results and based on voyage data, it has been reported that the remarkable fuel saving of up to 14% in trials and up to 30% in-service and rough weather by the container ship with the gate rudder system is greater than that of her sister ship, which was outfitted with a conventional rudder system (Sasaki, 2018, Tacar et al., 2020). In addition to fuel consumption reduction, improved motion characteristics, maneuvering and less propeller vibration have also been observed (Carchen et al., 2020). In 2020, the second and third applications of gate rudder were applied to two Japanese cargo vessels of 509 GT and 499 GT (Atlar, 2021). There is currently a new project named GATERS to apply the gate rudder system as a retrofit ship propulsion (Atlar, 2021).

The Gate Rudder System has a brief history and is still in development. A detailed review of the past numerical and experimental research of the Gate Rudder system has been presented by Tacar et al. (2020). A significant discrepancy in powering performance was found between the model test and the sea trial test of the first container ship with the gate rudder (Sasaki et al., 2020). The power savings in the sea trial of the container ship Shigenbou were more than the predictions based on the preliminary CFD analyses and model tests (Motorship 2019, Tacar et al. 2020). Sasaki and Atlar (2019) investigated the scale effect of the Gate Rudder system and concluded that the main reason for the discrepancy between the model test and full-scale data can be related to the scale effect associated with the drag and lift characteristics at low Reynolds numbers for both rudder blades. Tacar et al. (2020) numerically and experimentally investigate the gate rudder powering performance by using two different scale models for the same container ship.

Within the context of the preceding framework, the main objective is to investigate the propulsive performances of a model of a general cargo ship of 499 GT in three different scales (i.e., 3 m, 6 m, and full scale) fitted with conventional and gate rudder arrangements at full load and sea trial conditions. The other main objective of this analysis is to investigate the scale effects on the performance of the gate rudder system. The results obtained from CFD simulations have been compared and validated with experimental data of the model tests. The validated CFD results of the two model scales and ship scale have been compared to investigate the scale effect of the gate rudder performance. The numerical simulations for the study have been carried out in the RANSE-based commercial CFD solver Star CCM+.

In summary of the paper, the main particulars of the selected ship and its propeller have been discussed in Section 2. Section 3 consists of the details of the numerical analysis of the ship hull. The details of the formulation of the resistance and self-propulsion calculations have also been presented in Section 4. The results of calculated powering performances have been presented and discussed in Section 5. The resistance components were derived for two different scales along with a full-scale ship, and the scale effect on resistance is discussed in this section. Finally, the scale effect on the pressure distributions and velocity fields has also been presented in Section 5. In section 6, the main findings of the investigation have been summarized.

2 Main particulars and geometry of the selected ship

A domestic cargo ship was selected for the study. The cargo ship was fitted with both conventional and gate rudders. The geometry of the selected hull fitted with both types of rudders is shown in Fig. 2. The ship with gate rudder and conventional rudder were analyzed numerically with two different scaled models and full-scale ship. The ship was scaled with a scale factor of 1/11.5 and 1/23. Table 1 shows the principal particulars of the ship, as well as two different models with both rudder systems.

Table 1 Ship particulars

Particulars	Full Scale	Model 1	Model 2
Scale Factor	1	1/23	1/11.5
Length overall, m	74	3.22	6.43
Length between perpendiculars, m	69.0	3.0	6.0
Breadth, m	12.0	0.522	1.043
Draft, m	4.15	0.180	0.361
Depth, m	5.3	0.230	0.461
Block coefficient	0.72	0.72	0.72
Service Speed, m/s	6.687	1.394	1.972

Draft aft at trial, m	3.33	0.145	0.289
Draft fwd at trial, m	1.23	0.054	0.107
Block coefficient at trial	0.66	0.66	0.66
Propeller diameter, m			
Conventional Rudder	2.4	0.104	0.201
Gate Rudder	2.4	0.104	0.201
Propeller Hub Ratio	0.18	0.18	0.18

(a)

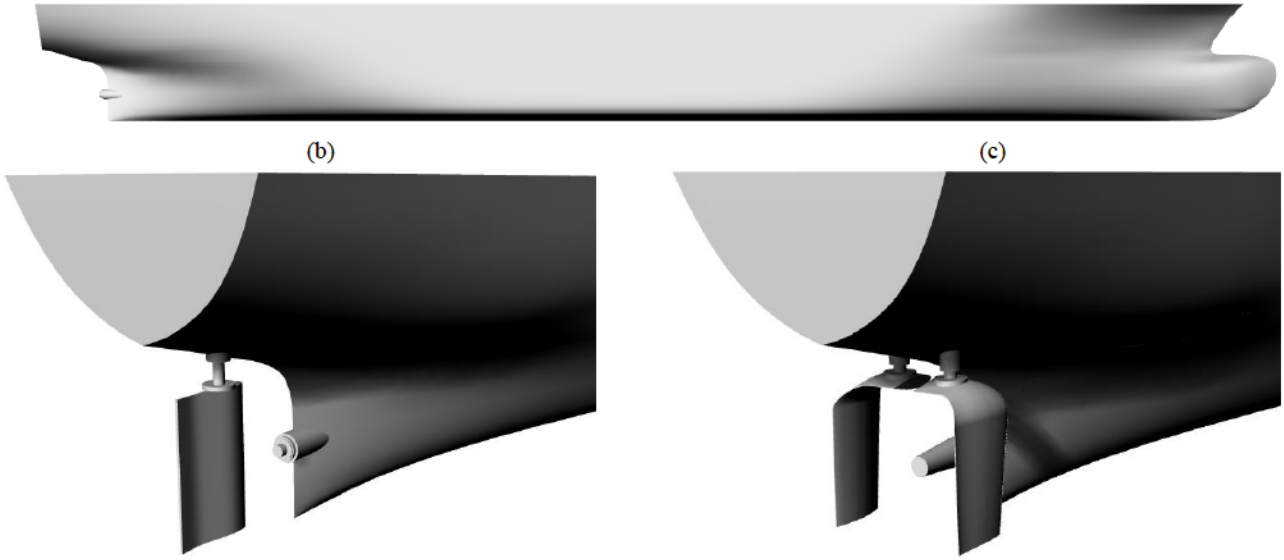

Fig. 2 (a) Ship profile (b) Ship stern part fitted with conventional rudder (c) Ship stern part fitted with gate rudder

3 Numerical Analysis

Resistance and propulsion characteristics of the ship fitted with conventional and gate rudders have been computed numerically. The numerical simulation has been carried out with commercial CFD solver Star CCM+ which solves the Unsteady Reynolds-Averaged Navier-Stokes (URANS) equations. Detailed formulations of numerical methods for CFD are well-known and thoroughly documented in a number of literatures. The most important aspects of the methods have been discussed in this section. The cases for the numerical predictions of the propulsive coefficients at various speeds in different scales at full load and sea trial conditions have been presented in Table 2.

Table 2 Numerical analysis matrix

Model	Simulation type	Rudder type	Loading condition and ship speed
Lpp=3 m	Resistance Test	No Rudder	Full load condition:
Lpp=6 m	Resistance Test	Conventional Rudder	10.97, 11.92, 12.95, 13.46 and 13.91
Lpp=69 m	Self-propulsion Test	Conventional Rudder	knots
	Resistance Test	Gate Rudder	Sea trial condition:
	Self-propulsion Test	Gate Rudder	11.5, 12.0 and 13.0 knots

3.1 Computational Fluid Dynamics (CFD) governing equations

Because the flow is incompressible and turbulent, the governing equations are the continuity equation and the momentum equations. The developed turbulent flow is quantitatively described using RANS equations and the time-averaged continuity equation.

Continuity equation and momentum equation can be written as,

$$\frac{\partial(\rho\bar{u}_i)}{\partial x_i} = 0 \quad (1)$$

$$\frac{\partial(\rho\bar{u}_i)}{\partial t} + \frac{\partial}{\partial x_j}\left(\rho\bar{u}_i\bar{u}_j + \rho\overline{u_i'u_j'}\right) = -\frac{\partial\bar{p}}{\partial x_i} + \frac{\partial\bar{\tau}_{ij}}{\partial x_j} \quad (2)$$

Where, ρ is the density, t is the time, $\bar{u}_i$ & $\bar{u}_j$ are the Cartesian components of velocity vector, $\bar{p}$ is the mean pressure and τ_{ij} is viscous stress tensor. The viscous stress tensors are defined as,

$$\bar{\tau}_{ij} = \mu\left(\frac{\partial\bar{u}_i}{\partial x_j} + \frac{\partial\bar{u}_j}{\partial x_i}\right) \quad (3)$$

Where, $\rho\overline{u_i'u_j'}$ is Reynolds Tensor Stress, $\bar{\tau}_{ij}$ is the mean viscous stress tensor, and μ is the dynamic viscosity. The selection of suitable turbulence modeling in unsteady fluid flow is an important aspect of CFD simulations of ships. Two variants of the k-ω model are implemented in STAR-CCM+ are Standard k-ω and SST k-ω. The advantage of the k-ω model over the k-ε model is that it performs better for boundary layers under adverse pressure gradients. Furthermore, the standard k-ω model can be used in this mode without the need for wall distance computation. The present study uses the two-equation SST k-ω turbulence model that solves turbulent kinetic energy transport equations.

3.2 CFD domain and boundary condition

Fig 3 shows the dimensions and the boundary conditions of the computational domains of the free-surface simulations of ship. ITTC recommended procedure for ship resistance and ship self-propulsion analyses through CFD were followed to select and chose the dimensions of the domain. Following the ITTC recommended procedure for ship CFD simulations (ITTC, 2014), inlet was defined 1.5 Lpp from FP and outlet 3 Lpp from AP. Bottom and top boundaries were taken 2.0 Lpp and 1.0 Lpp from the free surface respectively. Each side of the domain was taken 1.5 Lpp from the centerline. Symmetry conditions were considered with respect to vertical center plane in case of towing condition. The dimensions of the domain for all cases were kept same for respective two model scales. The hull surface was defined as no-slip wall type boundary condition. Inlet, top and bottom were defined as velocity inlet whereas the outlet defined as pressure outlet and sides were defined as slip symmetry boundary condition. Fig. 3 shows the domain and boundary conditions used throughout the simulations.

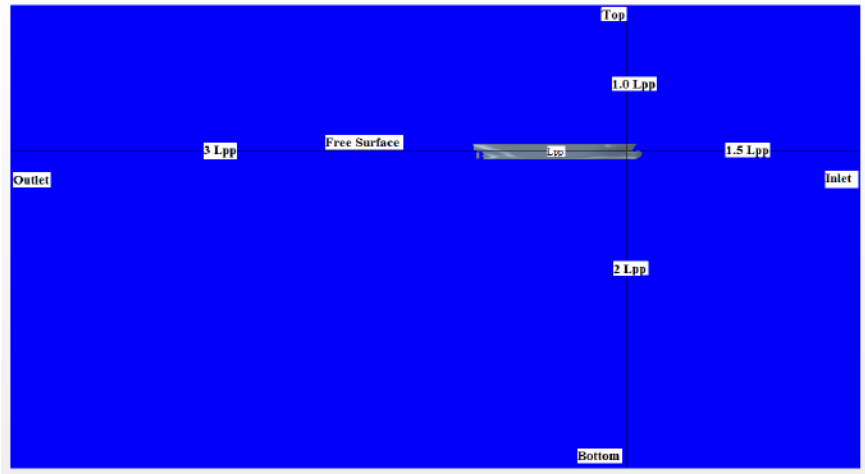

Fig. 3 Front view of CFD domain

3.3 Mesh generation and physics set up

The mesh generation was done using a trimmer type of mesh method, which is a STAR CCM+ built-in technique. The meshing technique used trimmed hexahedral grids and prism layers along the wall. The grid near the free surface was refined to capture the wave elevation precisely. Extra grid refinement was applied at the rudder region. In case of self-propulsion simulation,

extra refinement of the grid was done around the disk. There were six layers of boundary-layer meshes near the hull and the average wall function y+ value was kept between 30 and 60 as calculated and suggested by similar numerical studies. Fig 4 shows the generated volume mesh. SST k-ω turbulence model was used as the RANS closure model. The volume of fluid method (VOF) for multi-phase flows was used to account for free surface effects. The model was unconstrained to move in 2 degrees of freedom (with sinkage and trim) using Dynamic Fluid Body Interaction (DFBI), allowing the simulation to attain a consistent dynamic attitude for each speed run.

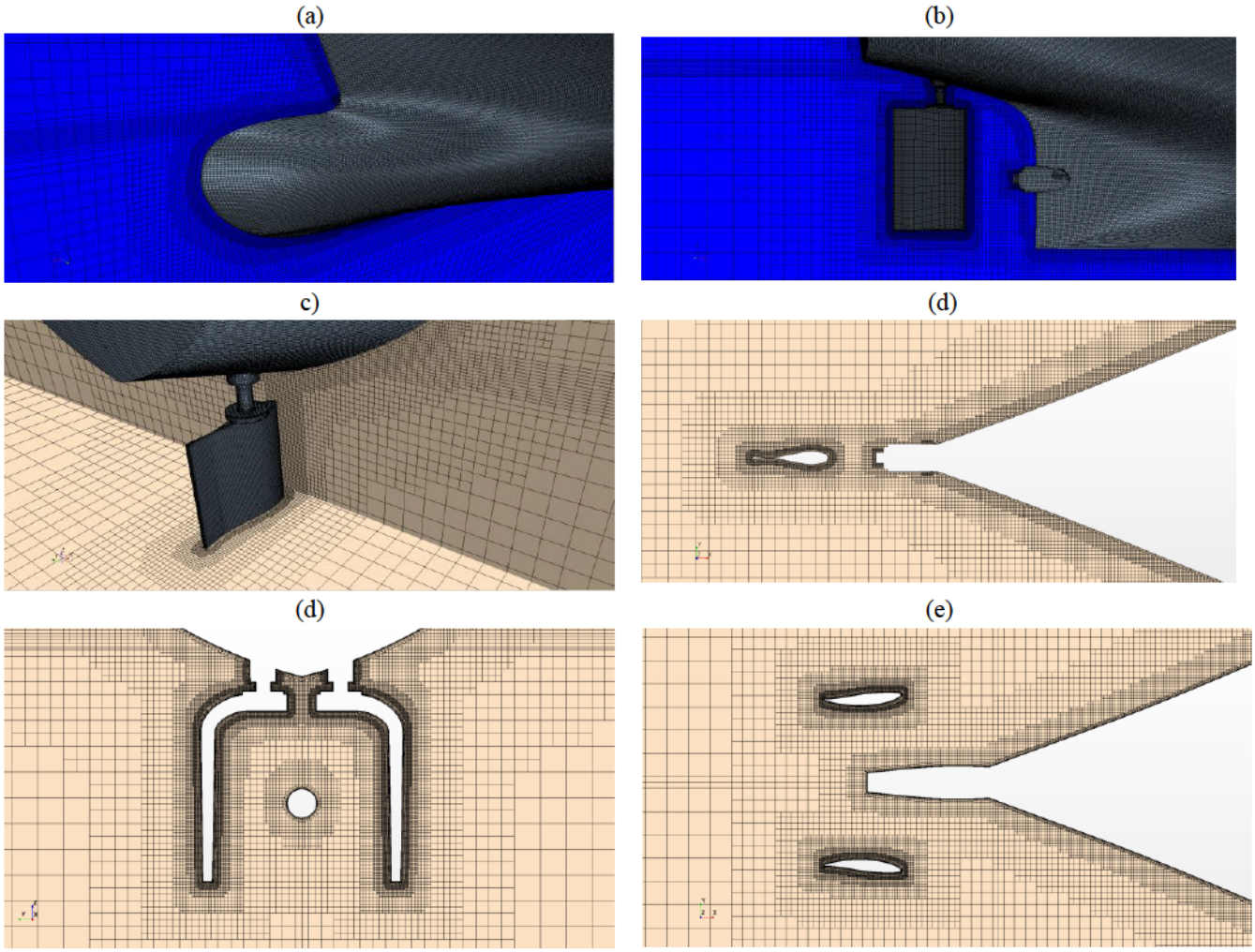

Fig 4. Generated volume mesh (a) at bow part of the hull (b) at the aft part of the hull with conventional rudder (c) mesh around conventional rudder (d) top view with conventional rudder (e) sectional view with gate rudder (f) top view with gate rudder

3.4 Grid Convergence, verification, and validation of numerical studies

The accuracy of the numerical results was checked by the uncertainty analysis based on iterative and grid convergence following guidelines of ITTC for uncertainty analysis of Ship CFD simulations. For this purpose, grid independency has been studied considering three different grid sizes for 6 m bare hull and the refinement ratio was taken $r_G = 1.30$ as recommended by ITTC (2017). Table 3 shows the results of grid convergence study of 6 m model which has been carried out following recommended procedure by ITTC for uncertainty analysis in CFD, verification and validation (ITTC, 2017). From the grid convergence study, it is observed that the relative error of the resistance decreases for finer grids. The relative error for the medium and fine mesh is below 2%. The level of verification of the study is relatively small (less than about 2.5%). Again, from Table 3 (c), it is seen that the value of error E%D is less than validation uncertainty U_V% S which indicates the

achievement of the validation for the simulations. The obtained average y+ value on the hull surface is about 35–40 which has been shown in Fig. 5. Symmetry condition was applied for the simulation of hull at towing to reduce the simulation time. The total number of mesh were approximately 1.0 M, 1.44 M, 2.07 M, 3.3 M, and 4.5 M for coarse to fine mesh respectively in case of 6 m model with conventional rudder. The total number of mesh was slightly higher in case of hull with gate rudder. Based on grid convergence study, base grid size for the medium mesh was taken for all the cases of the study. Total mesh number varied from 1.9–2.0 M for towing condition and 3.0–3.5 M for self-propulsion cases including mesh of virtual disk. The time step was chosen following ITTC recommendation. The time step must be less than 0.01 L/V when two equation turbulence model is used (ITTC, 2014). Hence time step was chosen 0.02 for 6 m model and 0.015 for 3 m model. Same physics set up was used for 3 m model simulation and the mesh size was scaled down by half of the 6 m model.

Table 3 Grid convergence and V&V study for the 6 m hull with conventional rudder resistance prediction; Fr No 0.256

(a) Grid convergence study: total resistance coefficients (C_T), frictional resistance coefficients (C_p) and pressure resistance coefficients (C_T)

Grids	h [mm]	#Cells	$C_T\times10^{-3}$	$\varepsilon\%\ S$	$C_F\times10^{-3}$	$\varepsilon\%S$	$C_F\times10^{-3}$ (ITTC)	$C_P\times10^{-3}$	$\varepsilon\%S$
Grid 1	65	1.0 M	4.449	-	2.851	-		1.598	-
Grid 2	50	1.4 M	4.328	2.72	2.839	0.56		1.493	6.57
Grid 3	39	2.0 M	4.263	1.50	2.825	0.35	2.972	1.438	3.68
Grid 4	30	3.3 M	4.211	0.99	2.817	0.28		1.404	2.42
Grid 5	20	4.5 M	4.207	0.33	2.812	0.18		1.395	0.65

(b) Verification of total resistance coefficients (C_T)

Grids	#Cells	$C_T\times10^{-3}$	P_G	C_G	U_G (%)	δ_G^*(%)	U_{GC} (%)	S_C
Grid 1–3	1.0 M	4.449	–	–	–	–	–	–
	1.4 M	4.328	–	–	–	–	–	–
	2.0 M	4.263	2.37	1.25	2.81	2.4	0.48	4.163
Grid 3–5	3.3 M	4.221	–	–	–	–	–	–
	4.5 M	4.207	2.68	1.57	0.35	0.55	0.20	3.978

(c) Validation of total resistance coefficients (C_T)

Grids	#Cells	$C_T\times10^{-3}$	EFD	E%D	$U_V\%\ S$	$U_V\%\ S_C$
Grid 1–3	1.0 M	4.449		2.46	–	–
	1.4 M	4.328		-0.33	–	–
	2.0 M	4.263	4.342	-0.94	2.76	2.41
Grid 3–5	3.3 M	4.221		-2.78	–	–
	4.5 M	4.207		-3.11	3.22	2.95

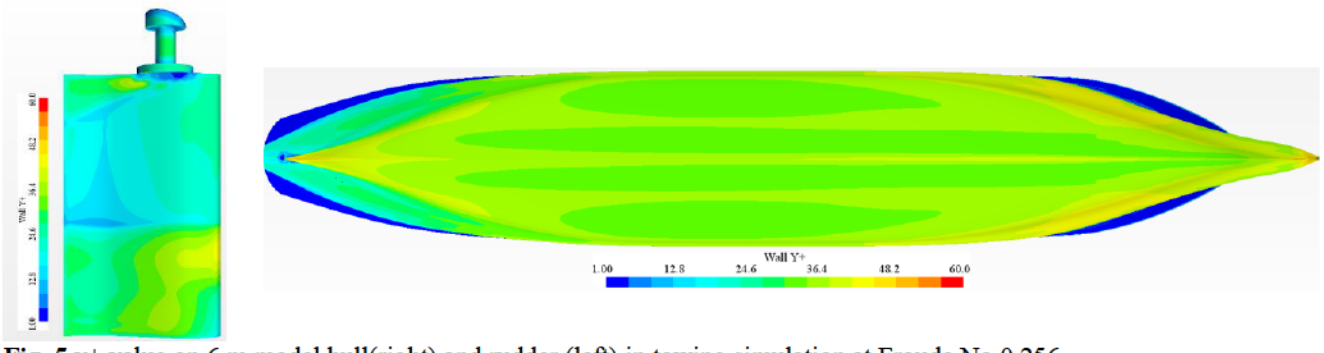

Fig. 5 y+ value on 6 m model hull(right) and rudder (left) in towing simulation at Froude No 0.256

Three different grid numbers have been taken for the study of full-scale ship and the total number of grids are about 7.0 M, 10.0 M, and 14.0 M for coarse, medium and fine mesh respectively. The meshes were generated applying a similar method of

model scale with the refinement ratio $r_G = 1.40$. Table 4 shows the uncertainty analysis of the ship with gate rudder in full scale for Froude No 0.264. δ_G^* and U_{GC} are 2.32 % and 2.16 % of corrected simulation value *Sc*, respectively. In both cases, the level of verification is below 2.5% which can be considered relatively small. The size of the time step for the full the scale simulations was taken 0.002Lpp/V. The average y+ value on the hull is about 200 as shown in Fig. 6 and the range is reasonable for the full-scale simulations. Medium mesh (~10 M) has been chosen for the study of full-scale simulations of the ship based on the uncertainty analysis.

Table 4 Grid convergence and V&V study for the full-scale ship with gate rudder towing; Fr No 0.264

(a) Grid Convergence Study

Grid	#Cells	$C_T \times 10^{-3}$	$\varepsilon\% S$	$C_F \times 10^{-3}$	$\varepsilon\% S$	$C_F \times 10^{-3}$ (ITTC)	$C_P \times 10^{-3}$	$\varepsilon\% S$
Coarse(S_3)	7.0 M	3.522	–	1.781	–	1.729	1.741	–
Medium (S_2)	10.0 M	3.386	4.02	1.756	1.42		1.633	6.66
Fine (S_1)	14.0 M	3.314	2.17	1.739	0.98		1.585	3.02

(b) Verification of total resistance

Grid	#Cells	$C_T \times 10^{-3}$	P_G	C_G	U_G (%)	δ_G^*(%)	U_{GC} (%)	S_C
Coarse(S_3)	7.0 M	3.522	–	–	–	–	–	–
Medium (S_2)	10.0 M	3.386	–	–	–	–	–	–
Fine (S_1)	14.0 M	3.314	1.89	0.93	2.44	2.32	2.16	3.239

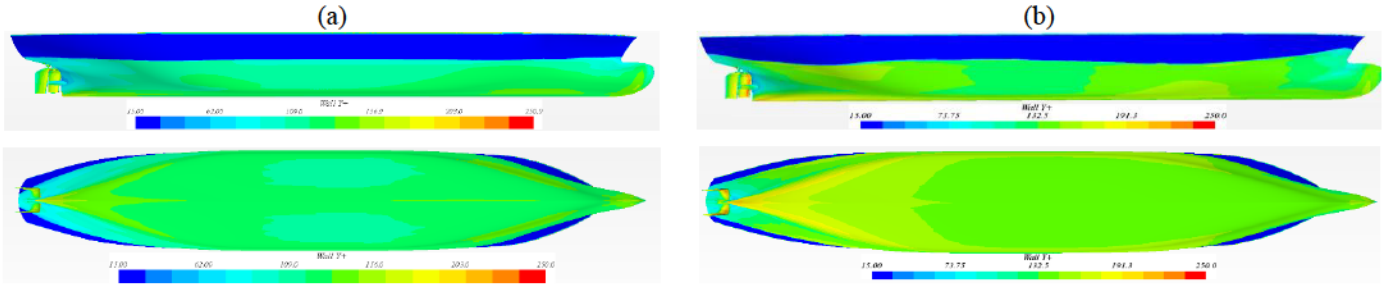

Fig. 6 y+ value on full scale ship hull at Froude No 0.2664 (a) Towing simulation (b) Self-propelled simulation

4.0 Resistance and powering calculation

Total resistance, R_T acting on ship obtained from numerical simulation can be divided into two components: frictional resistance, R_F and pressure resistance, R_P.

$$R_T = R_F + R_P \quad (4)$$

The resistance value can be non-dimensionalized by dividing dynamic pressure which is equivalent to $0.5\rho SV^2$. The equation (4) can be written in non-dimensionalized form as,

$$C_T = C_F + C_P \quad (5)$$

Where, C_T is total resistance coefficient, C_F is frictional resistance coefficient and C_P is pressure resistance coefficient. As the resistance tests are simulated in model scale, these are required to extrapolate in full scale. Form factor (1+k) values are required to extrapolate the model test results into full scale. The form factor can be computed from the resistance obtained from a CFD computation with flat-free surface simulated with symmetry boundary conditions at the proper Reynolds number. The form factor (1+k) is defined as,

$$(1 + k) = C_{TM}/C_{FM} \quad (6)$$

Where, C_{TM} is taken from CFD computation and C_{FM} is calculated by using ITTC 1957 formula (ITTC, 2014). The values of (1+k) used in this calculation have been presented in Table 5 and obtained based on model experiment. The residuary resistance coefficient can be obtained from total resistance obtained by CFD using form factor.

$$C_{RM} = C_{RS} = C_{TM} - C_{VM} = C_{TM} - (1+k)C_{FM} \quad (7)$$

Now the total ship resistance can be obtained by using the following equation (8),

$$C_{TS} = (1+k)C_{FS} + C_{RS} + \Delta C_F + C_{AA} \quad (8)$$

Here, ΔC_F is the roughness allowance factor which depends on Reynolds Number and is calculated using equation (9). Ship frictional resistance coefficient C_{FS} is calculated using ITTC 1957 formula.

$$\Delta C_F = 0.044\left[\left(\frac{k_s}{L_{WL}}\right)^{\frac{1}{3}} - 10\,Re^{-\frac{1}{3}}\right] + 1.25\times10^{-4} \quad (9)$$

Where, k_s is the surface roughness and the IITC recommended value is $150\times10^{-6}\ m$. In above equations subscript s represents for ship and m represents model.

Table 5 Form Factors (1+k)

Loading Condition	Scale	(1+k)
Full Load Condition	11.5	1.35
	23.0	1.30
Sea Trial Condition	11.5	1.33
	23.0	1.28

In the self-propulsion simulation, the geometry of the propeller was not modelled alongside the hull, but rather virtual disk model was implemented using experimental propeller open-water performance data. The propeller open water curves have been represented in Fig 7(a) and Fig 7(b) and are used in this study. The gate rudder system can be regarded as the ducted propeller. Therefore, the propeller design is quite different from a conventional propeller design. General trends of the propeller of gate rudder system are: a) 5–10% smaller than the conventional propeller and b) higher pitch ratio reflecting the higher flow speed (Sasaki et al., 2018). The propeller open water curves are quite different from the above reasons.

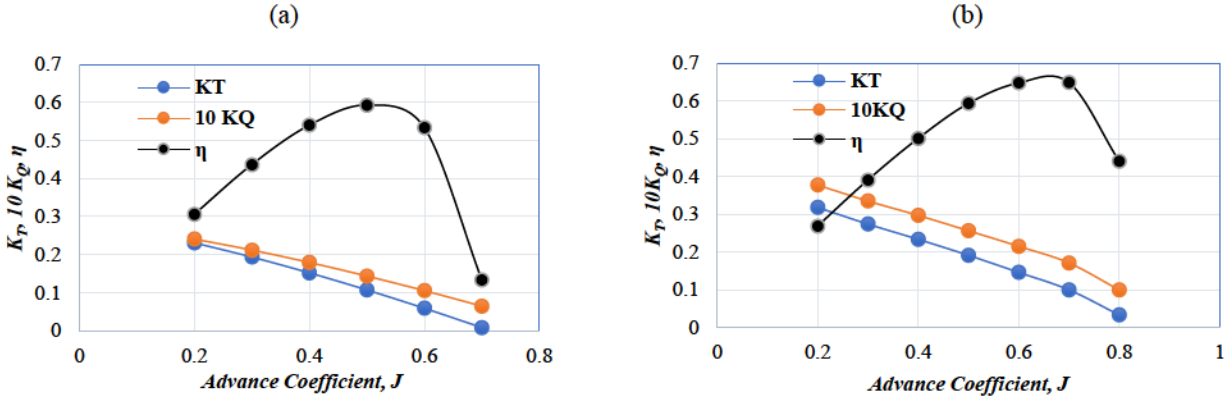

Fig. 7 Propeller open water curves (a) propeller with converntional rudder (b) propeller with gate rudder

The propeller performance parameters are expressed by,

$$K_T = \frac{T}{\rho n^2 D^4} \quad (10a)$$

$$K_Q = \frac{Q}{\rho n^2 D^5} \quad (10b)$$

$$J = \frac{V_a}{nD} \quad (10c)$$

Where, K_T and K_Q are the thrust coefficients and torque coefficients of virtual disk respectively, T is the thrust produced by virtual disk, Q is the torque, n is the rotation rate in per second, D is the virtual disk diameter. The self-propulsion computation requires finding the point at which ship resistance and propeller thrust are in equilibrium, i.e., it must fulfill the criteria $R_{T(SP)}-T=0$. As the computation has been performed in model scale and it is required to extrapolate in full scale, then a skin friction correction factor (SFC) must be added to the thrust to account for the reduction of resistance due to friction in full scale compared to scale.

$$SFC = 0.5\,\rho S V^2\{(1+k)(C_{FM} - C_{FS}) - \Delta C_F\} \quad (11)$$

Where, T is the thrust generated by the virtual disk, $R_{T\,(SP)}$ is the resistance at self-propelled condition and SFC is the Skin Friction Correction. Thus, the self-propulsion point is obtained fulfilling the criteria $T = R_{T\,(SP)} - SFC$ varying propeller rotation rate at a constant ship speed or varying inlet velocity at a constant propeller rotation rate. In this analysis, the inlet velocity was kept constant while the virtual disk rotation was varied to obtain ship self-propulsion point using force balanced method. It can be mentioned that this analysis has been performed for both model and ship propulsion point. The propulsion factors were obtained using torque identity method recommended by ITTC. The thrust deduction factor, t is calculated by,

$$t = \frac{R_{T,sp} - R_{T,tow}}{T} \quad (12)$$

Where $R_{T,sp}$ the resistance of the model ship is at self-propelled condition and $R_{T,tow}$ is the resistance of the model ship at towing condition. The thrust deduction factor, t for unconventional propulsion system, such as gate rudder system is recommended by ITTC (2014) as follow:

$$t = \frac{R_{T,sp} + T_{GR} - R_{T,tow}}{T + T_{GR}} \quad (13)$$

The wake fraction, w is calculated by:

$$w = \frac{V_m - V_a}{V_m} = 1 - \frac{J_m D_m n_m}{V_m} \quad (14)$$

Where, V_a is the velocity of advance which is taken as average axial velocity at the virtual disk and V_m is the model velocity. According to ITTC recommendation, V_a is the propeller open water advance speed which has been obtained using propeller open water curves based on thrust identity method in this calculation knowing the propeller rotation rate n_m from self-propulsion simulations. Analyzing the effective wake of a ship with gate rudder system is one of the difficult parts, as advance speed of the propeller is accelerated by the gate rudder blade which is not the component of effective wake (Sasaki et al., 2020). In case of gate rudder system, the rudder is not placed in the slipstream of the propeller and the flow field around the gate rudder is uniform. Induced velocity of the gate rudder blades is the main reason of the difference of the effective wake at the propeller plane with and without gate rudder. Because of the low Reynolds number at model scales, flow regimes around the gate rudder can be laminar (Turkmen et al., 2016). Thus, the effective wake obtained by a model with gate rudder cannot be scaled to full scale ship applying the method that is used in the conventional rudder case (Sasaki et al. 2020). The following expression has been proposed by Sasaki et al. (2020) to predict the nondimensional mean flow speed at the propeller plane of the gate rudder system,

$$v_p = C_1 v_{A0} + v_{inP} + V_{inR} \quad (16)$$

where, v_{A0} is the propeller advance speed of the conventional rudder, v_{inP} is propeller induced velocity and v_{inR} is rudder induced velocity. C_1 is a correlation factor of the wake variation which is assumed less than 1 due to the smaller propeller thrust and smaller propeller diameter of gate rudder system. The expression of effective wake of a ship with gate rudder arrangement can be written from Equation (16) as follow (Sasaki et al., 2020),

$$w_{GR} = C_1 \times (w_0 - 0.04) + w_{inR} \tag{17}$$

where, w_{inR} is rudder induced wake and the mean value can be obtained using the following expression (Sasaki et al., 2020),

$$w_{inR} = C_2 \times C_T + w_{0R} \tag{18}$$

where, C_2 denotes the correction factor for the thrust loading. Fig. 8 shows typical schematic of the scale effect of the wake of a gate rudder propulsion system. In this figure, dotted line represents the scale effects of conventional rudder and solid line represents the scale effects of gate rudder system. According to the ITTC recommended approach, the point A' may be predicted from the point A whereas the point B' is not bound by the same principles, and B' can occasionally be smaller than the point B, as illustrated in Fig. 8 (Sasaki et al., 2020). Therefore, full scale ship data with gate rudder is required to evaluate presented wake scaling procedure which shows a slightly better result for gate rudder compared with ITTC procedure.

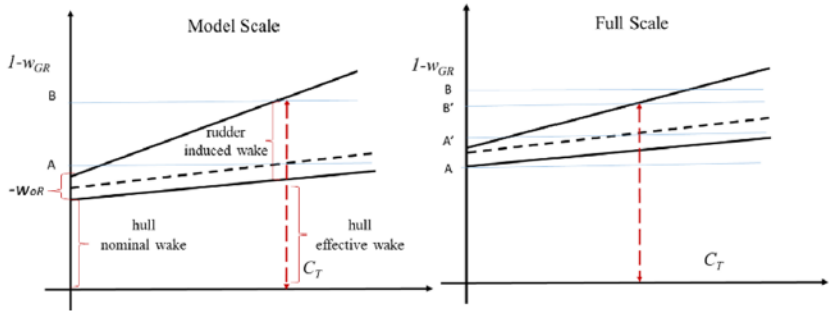

Fig. 8 Schematic of the scale effect of the wake of a gate rudder propulsion system (Sasaki et. al, 2020)

The velocity advance coefficient J, open water efficiency η_o and relative rotative efficiency η_R are found based on thrust identity method using propeller open water curves. The following expressions are used for details powering calculations.

$$\eta_o = \frac{J}{2\pi}\frac{K_T}{K_Q} \tag{19a}$$

$$\eta_R = \frac{K_{Qo}}{K_Q} \tag{19b}$$

$$\eta_D = \eta_o\, \eta_H\, \eta_R = \frac{P_E}{P_D} \tag{19c}$$

$$P_B = P_D/\eta_t \tag{19d}$$

The fuel oil consumption (FOC) in ton per day can be calculated by,

$$FOC = \frac{24 \times FOCR \times P_B}{10^6} \tag{20}$$

Where, FOCR is Fuel Oil Consumption Rate which is taken 200 g/kw/h for marine diesel engine and transmission efficiency η_t is taken as 0.97 – 0.99. For domestic vessels, it is taken 0.97 and this value is used in the study.

5 Results and Discussion

Numerical analyses were conducted for two model scales at various speeds with two loading conditions, i.e., full load and sea trial conditions and for full scale at various speeds in full load condition. Frictional resistance and residual resistance were calculated using free surface simulations. The results of resistance obtained from CFD simulations for model scales have been extrapolated to full scale to investigate the scale effects and detailed powering calculation have been carried out following ITTC recommended procedure as described in the previous section. The summary of the extrapolated results with the propulsive factors and powering calculations obtained by both model scales of the ship with conventional and gate rudder in full load condition has been shown in Tables 6–9. The tabulated self-propelled data is presented at ship propulsion point. In the tables, *Re* denotes Reynolds number, C_T total resistance coefficient and C_F frictional resistance coefficient. The subscript *m* indicates the model and *s* indicated the ship. In the tables, *Rrud* represents the rudder resistance contributed by the conventional rudder and *Trud* represents the thrust generated by the gate rudder which was originally the negative resistance in CFD simulations contributed by gate rudder. The propulsive factors, i.e., thrust deduction factor, *t* and wake fraction, *w* is calculated using the formulae mention in Section 4. The open water efficiency η_0 and relative rotative efficiency η_R have been estimated based on thrust identity method, a standard procedure recommended by ITTC.

From the tables, it is observed that the total resistance coefficients of the ship hull with gate rudder are greater than ship hull with conventional rudder. The frictional resistance seems to be about similar for both cases of rudder for a particular model scale as expected but the variations are due for pressure resistances. The friction resistance coefficients obtained by CFD and predicted by ITTC shows good agreement in both model scales as shown in Fig. 9. The total resistance coefficients obtained by 3 m model are higher than the value obtained by 6 m model. In these tables, the thrust deduction factors in case of ship fitted with conventional rudder obtained by both model scale is about 0.17 – 0.20 whereas, the value is about 0.09– 0.11 in case of gate rudder. The wake fraction value is about 0.35 – 0.38 in case of conventional rudder and it is about 0.20 – 0.24 in case of gate rudder. The hull efficiencies obtained in various speed with conventional rudder are about 1.23 – 1.30 in case of ship fitted with conventional rudder, whereas the range is 1.14–1.18 in case of both model scales. The delivered power P_D is estimated using quasi-propulsive efficiency η and the shaft efficiency is assumed as 0.99 to calculate the brake power. The quasi-propulsive efficiency tends to higher for ship with gate rudder compared to ship with gate rudder and it has increased with the larger scale model. It can be mentioned that both thrust deduction factor and wake fraction have been assumed equal for ship and model to the brake power calculation.

Table 6 Summary of resistance and powering calculations predicted by 3 m Hull with Conventional Rudder by CFD, Full load condition at ship propulsion point

(a) Towing simulations

Vm(m/s)	Froude No	Rem	$C_{TM}\times10^{-3}$ (Bare Hull)	R_{TM} (N) (Hull with CR)	$C_{TM}\times10^{-3}$ (Hull with CR)	$C_{FM}\times10^{-3}$ (Hull With CR)	$C_{PM}\times10^{-3}$ (Hull With CR)
1.177	0.2084	3.16E+06	4.601	6.761	4.600	3.625	0.975
1.279	0.2265	3.43E+06	4.644	8.081	4.657	3.547	1.110
1.389	0.2461	3.73E+06	4.835	9.987	4.876	3.487	1.389
1.444	0.2557	3.87E+06	5.167	11.552	5.221	3.478	1.743
1.492	0.2644	4.00E+06	5.580	13.297	5.627	3.440	2.187

(b) Self-propulsion simulation at ship propulsion point

Froude No	R_{TM} (N)	$C_{TM}\times10^{-3}$	$C_{FM}\times10^{-3}$	$C_{FM}\times10^{-3}$ (ITTC)	SFC (N)	Rrud (N)	n (rps)	T (N)	Q (N-m)	K_T	K_Q
0.2084	7.502	5.308	3.649	3.705	2.3	0.241	16.0	5.50	0.0788	0.181	0.025
0.2265	9.001	5.362	3.572	3.646	2.64	0.302	18.1	6.66	0.0757	0.173	0.019
0.2461	11.136	5.760	3.551	3.589	3.04	0.456	20.0	8.75	0.1182	0.184	0.024
0.2557	12.607	6.023	3.539	3.563	3.25	0.406	21.5	10.10	0.1204	0.176	0.0201
0.2644	14.715	6.479	3.487	3.541	3.43	0.490	22.7	11.88	0.1495	0.174	0.021

(c) Resistance extrapolation to full scale

Froude No	Vm (m/s)	Vs (m/s)	Rem	Res	$C_{FS}\times10^{-3}$	$C_{RM}\times10^{-3}=C_{RS}\times10^{-3}$	ΔC_F	$C_{TS}\times10^{-3}$	R_T (kN)

0.2084	1.177	5.643	3.16E+06	3.33E+08	1.763	0.564	0.713	3.569	65.42
0.2265	1.279	6.132	3.43E+06	3.62E+08	1.744	0.719	0.713	3.699	80.05
0.2461	1.389	6.661	3.73E+06	3.93E+08	1.725	1.144	0.713	4.100	104.70
0.2557	1.444	6.924	3.87E+06	4.08E+08	1.716	1.422	0.713	4.366	120.46
0.2644	1.492	7.155	4.00E+06	4.22E+08	1.709	1.946	0.713	4.880	143.79

(d) Propulsive factors, powering, and fuel oil consumption calculation

Froude No	Vs (m/s)	t	w	η_H	η_o	η_R	η	P_E (kW)	P_D (kW)	P_B (kW)	FOC (ton/day)
0.2084	5.643	0.189	0.394	1.338	0.546	0.991	0.697	369.1	530	546	2.622
0.2265	6.132	0.183	0.381	1.320	0.523	0.996	0.687	490.8	726	749	3.593
0.2461	6.661	0.206	0.375	1.271	0.544	0.991	0.686	697.5	1017	1049	5.034
0.2557	6.924	0.178	0.379	1.324	0.534	1.004	0.710	834.0	1175	1211	5.815
0.2644	7.155	0.179	0.376	1.299	0.527	1.007	0.689	1028.9	1494	1540	7.393

Table 7 Summary of resistance and powering calculations predicted by 3 m Hull with Gate Rudder by CFD, Full load condition at ship propulsion point

(a) Towing simulations

Vm(m/s)	Froude No	Rem	$C_{TM} \times 10^{-3}$ (Bare Hull)	R_{TM} (N) (Hull with GR)	$C_{TM} \times 10^{-3}$ (Hull with GR)	$C_{FM} \times 10^{-3}$ (Hull With GR)	$C_{PM} \times 10^{-3}$ (Hull With GR)
1.177	0.2084	3.16E+06	4.601	7.017	4.702	3.647	1.055
1.279	0.2265	3.43E+06	4.644	8.332	4.728	3.570	1.158
1.389	0.2461	3.73E+06	4.835	10.334	4.969	3.522	1.447
1.444	0.2557	3.87E+06	5.167	11.803	5.253	3.501	1.752
1.492	0.2644	4.00E+06	5.580	13.749	5.729	3.476	2.253

(b) Self-propulsion simulation at ship propulsion point

Froude No	R_{TM} (N)	$C_{TM} \times 10^{-3}$	$C_{FM} \times 10^{-3}$	$C_{FM} \times 10^{-3}$ (ITTC)	SFC (N)	Rrud (N)	n (rps)	T (N)	Q (N-m)	K_T	K_Q
0.2084	7.017	5.105	3.637	3.705	2.3	0.207	15.32	5.199	0.070	0.187	0.024
0.2265	8.332	5.187	3.582	3.646	2.64	0.236	15.77	6.339	0.089	0.190	0.025
0.2461	10.334	5.437	3.539	3.589	3.04	0.277	16.72	8.097	0.110	0.195	0.025
0.2557	11.803	5.698	3.511	3.563	3.25	0.338	19.91	9.358	0.125	0.199	0.025
0.2644	13.749	6.227	3.480	3.541	3.43	0.461	21.32	11.281	0.150	0.210	0.027

(c) Resistance extrapolation to full scale

Froude No	Vm (m/s)	Vs (m/s)	Rem	Res	$C_{FS} \times 10^{-3}$	$C_{RM} \times 10^{-3} = C_{RS} \times 10^{-3}$	ΔC_F	$C_{TS} \times 10^{-3}$	R_T (kN)
0.2084	1.177	5.643	3.16E+06	3.33E+08	1.763	0.377	0.713	3.382	61.98
0.2265	1.279	6.132	3.43E+06	3.62E+08	1.744	0.531	0.713	3.511	75.98
0.2461	1.389	6.661	3.73E+06	3.93E+08	1.725	0.837	0.713	3.792	96.85
0.2557	1.444	6.924	3.87E+06	4.08E+08	1.716	1.134	0.713	4.077	112.50
0.2644	1.492	7.155	4.00E+06	4.22E+08	1.709	1.704	0.713	4.638	136.67

(d) Propulsive factors, powering, and fuel oil consumption calculation

Froude No	Vs (m/s)	t	w	η_H	η_o	η_R	η	P_E (kW)	P_D (kW)	P_B (kW)	FOC (ton/day)
0.2084	5.643	0.102	0.24	1.182	0.582	0.997	0.686	349.8	510	526	2.525
0.2265	6.132	0.117	0.234	1.153	0.582	0.976	0.655	465.9	711	733	3.519
0.2461	6.661	0.108	0.243	1.178	0.571	0.988	0.665	645.2	970	1000	4.799
0.2557	6.924	0.099	0.234	1.176	0.582	0.998	0.683	778.9	1140	1175	5.639
0.2644	7.155	0.105	0.2244	1.155	0.589	0.999	0.679	977.9	1440	1485	7.128

Table 8 Summary of resistance and powering calculations predicted by 6 m Hull with Conventional Rudder by CFD, Full load condition at ship propulsion point

(a) Towing simulations

Vm(m/s)	Froude No	Rem	$C_{TM}\times10^{-3}$ (Bare Hull)	R_{TM} (N) (Hull with CR)	$C_{TM}\times10^{-3}$ (Hull with CR)	$C_{FM}\times10^{-3}$ (Hull With CR)	$C_{PM}\times10^{-3}$ (Hull With CR)
1.664	0.2084	8.93E+06	3.769	42.229	3.797	2.842	0.955
1.808	0.2265	9.70E+06	3.814	53.989	3.895	2.853	1.042
1.964	0.2461	1.05E+07	4.159	69.526	4.249	2.839	1.410
2.042	0.2557	1.10E+07	4.583	82.643	4.675	2.839	1.836
2.110	0.2644	1.13E+07	5.193	99.692	5.281	2.827	2.454

(b) Self-propulsion simulation at ship propulsion point

Froude No	R_{TM} (N)	$C_{TM}\times10^{-3}$	$C_{FM}\times10^{-3}$	$C_{FM}\times10^{-3}$ (ITTC)	SFC (N)	Rrud (N)	n (rps)	T (N)	Q (N-m)	K_T	K_Q
0.2084	50.29	4.411	2.986	3.060	9.95	2.7	14.40	40.35	1.71	0.178	0.021
0.2265	64.64	4.908	2.963	3.016	11.39	3.69	15.64	53.25	1.94	0.179	0.020
0.2461	83.65	5.333	2.942	2.973	13.02	4.85	17.00	70.63	2.284	0.178	0.020
0.2557	99.84	5.792	2.925	2.953	13.86	5.19	17.66	85.98	2.51	0.182	0.020
0.2644	120.96	6.465	2.911	2.936	14.62	5.87	18.25	106.34	2.66	0.181	0.020

(c) Resistance extrapolation to full scale

Froude No	Vm (m/s)	Vs (m/s)	Rem	Res	$C_{FS}\times10^{-3}$	$C_{RM}\times10^{-3}=C_{RS}\times10^{-3}$	ΔC_F	$C_{TS}\times10^{-3}$	R_T (kN)
0.2084	1.664	5.643	8.93E+06	3.33E+08	1.763	0.380	0.713	3.473	63.65
0.2265	1.808	6.132	9.70E+06	3.62E+08	1.744	0.908	0.713	3.975	86.01
0.2461	1.964	6.661	1.05E+07	3.93E+08	1.725	1.361	0.713	4.402	112.42
0.2557	2.042	6.924	1.10E+07	4.08E+08	1.716	1.843	0.713	4.872	134.43
0.2644	2.110	7.155	1.13E+07	4.22E+08	1.709	2.536	0.713	5.555	163.69

(d) Propulsive factors, powering, and fuel oil consumption calculation

Froude No	Vs (m/s)	t	w	η_H	η_o	η_R	η	P_E (kW)	P_D (kW)	P_B (kW)	FOC (ton/day)
0.2084	5.643	0.186	0.357	1.267	0.549	0.990	0.688	359	522	538	2.582
0.2265	6.132	0.208	0.357	1.232	0.559	1.000	0.689	527	766	790	3.790
0.2461	6.661	0.204	0.353	1.230	0.567	0.990	0.690	749	1085	1119	5.370
0.2557	6.924	0.194	0.363	1.266	0.566	0.990	0.709	931	1313	1354	6.498
0.2644	7.155	0.184	0.363	1.281	0.558	0.990	0.708	1171	1655	1706	8.189

Table 9 Summary of resistance and powering calculations predicted by 6 m Hull with Gate Rudder by CFD, Full load condition at ship propulsion point

(a) Towing simulations

Vm(m/s)	Froude No	Rem	$C_{TM}\times10^{-3}$ (Bare Hull)	R_{TM} (N) (Hull with GR)	$C_{TM}\times10^{-3}$ (Hull with GR)	$C_{FM}\times10^{-3}$ (Hull With GR)	$C_{PM}\times10^{-3}$ (Hull With GR)
1.664	0.2084	8.93E+06	3.769	45.556	3.867	2.953	0.913
1.808	0.2265	9.70E+06	3.814	58.404	4.198	2.910	1.289
1.964	0.2461	1.05E+07	4.159	74.765	4.554	2.895	1.658
2.042	0.2557	1.10E+07	4.583	86.971	4.903	2.894	2.009
2.110	0.2644	1.13E+07	5.193	105.477	5.568	2.872	2.696

(b) Self-propulsion simulations at ship propulsion point

Froude No	R_{TM} (N)	$C_{TM}\times10^{-3}$	$C_{FM}\times10^{-3}$	$C_{FM}\times10^{-3}$ (ITTC)	SFC (N)	Rrud (N)	n (rps)	T (N)	Q (N-m)	K_T	K_Q
0.2084	46.95	3.985	2.963	3.060	9.95	1.547	11.5	36.998	1.345	0.167	0.021
0.2265	61.45	4.417	2.913	3.016	11.39	2.036	13.6	50.056	1.900	0.162	0.022
0.2461	79.39	4.736	2.883	2.973	13.02	2.668	15.5	66.374	2.432	0.165	0.023

0.2557	91.72	5.171	2.865	2.953	13.86	3.335	16.6	77.865	2.810	0.169	0.023
0.2644	110.69	5.843	2.852	2.936	14.62	4.485	18.1	96.072	3.318	0.175	0.024

(c) Resistance extrapolation to full scale

Froude No	Vm (m/s)	Vs (m/s)	Rem	Res	$C_{FS}\times10^{-3}$	$C_{RM}\times10^{-3}=C_{RS}\times10^{-3}$	ΔC_F	$C_{TS}\times10^{-3}$	R_T (kN)
0.2084	1.664	5.643	8.93E+06	3.33E+08	1.763	0.380	0.713	3.078	56.41
0.2265	1.808	6.132	9.70E+06	3.62E+08	1.744	0.322	0.713	3.552	76.86
0.2461	1.964	6.661	1.05E+07	3.93E+08	1.725	0.696	0.713	3.885	99.23
0.2557	2.042	6.924	1.10E+07	4.08E+08	1.716	1.048	0.713	4.332	119.54
0.2644	2.110	7.155	1.13E+07	4.22E+08	1.709	1.742	0.713	5.012	147.70

(d) Propulsive factors, powering, and fuel oil consumption calculation

Froude No	Vs (m/s)	t	w	η_H	η_o	η_R	η	P_E (kW)	P_D (kW)	P_B (kW)	FOC (ton/day)
0.2084	5.643	0.094	0.219	1.160	0.594	0.973	0.670	318	475	490	2.351
0.2265	6.132	0.097	0.219	1.156	0.605	0.978	0.684	471	689	710	3.407
0.2461	6.661	0.096	0.220	1.159	0.589	0.980	0.669	661	989	1019	4.892
0.2557	6.924	0.100	0.220	1.154	0.600	0.987	0.683	828	1212	1249	5.996
0.2644	7.155	0.106	0.217	1.147	0.602	0.973	0.660	1057	1581	1630	7.824

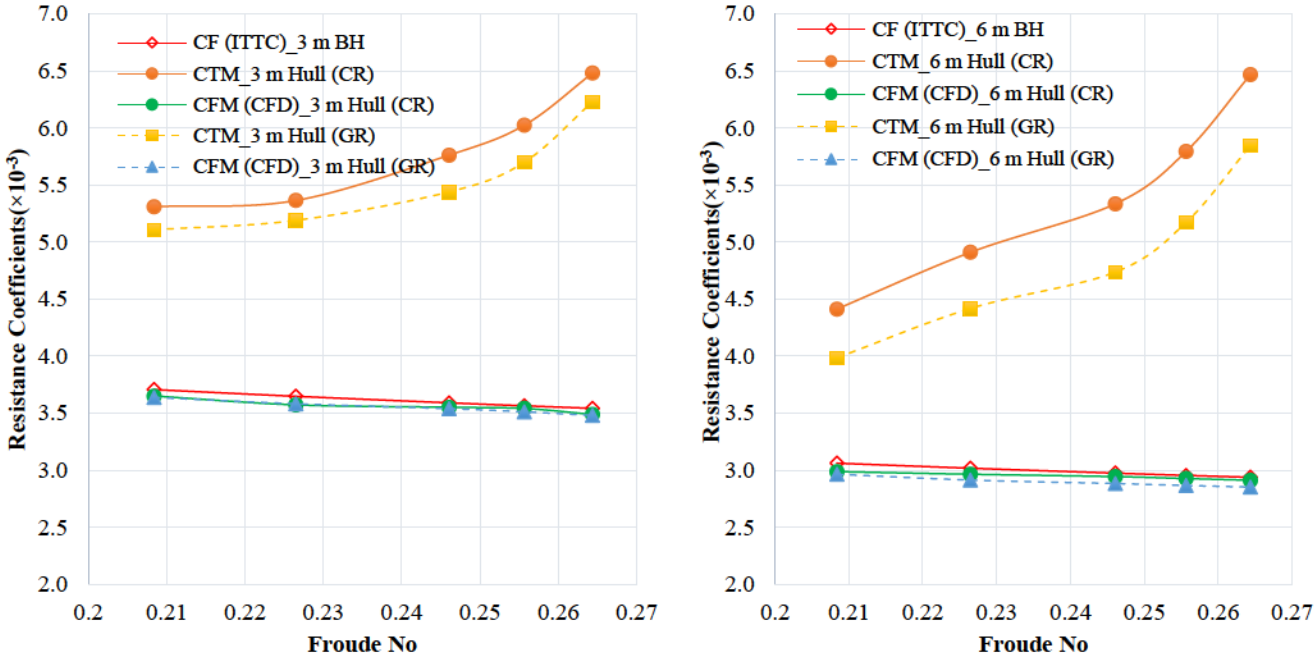

Fig. 9 Resistance coefficients of model with self-propulsion at full load condition obtained by CFD

Figs. 10 and 11 demonstrate the scale effects on the resistance of the ship hull with conventional and gate rudders. Figs. 10 (a) and (c) show total resistance obtained by 3 m and 6 m models with the conventional rudder, respectively. Figs. 10 (b) and (d) show total resistance obtained by 3 m and 6 m models with the gate rudder, respectively. From the figures, it is seen that the reduction in total resistance of the ship with gate rudder compared to conventional rudder varies from 6–8 % in the case of prediction by the 3 m hull and 9–12% in the case of the 6 m hull, which indicates there is a strong influence of scale effects in gate rudder thrust generation. In Fig. 11(a), total resistance at self-propulsion with a service speed of 13 kts is approximately 104.7 kN for the 3 m model with conventional rudder, whereas the value is approximately 97.40 kN for the 3 m model with gate rudder. Again in Fig. 11 (b), total resistance at self-propelled condition at service speed is about 112.4 kN obtained by 6 m model with conventional rudder, whereas the value is about 101.8 kN obtained by 6 m model with gate rudder.

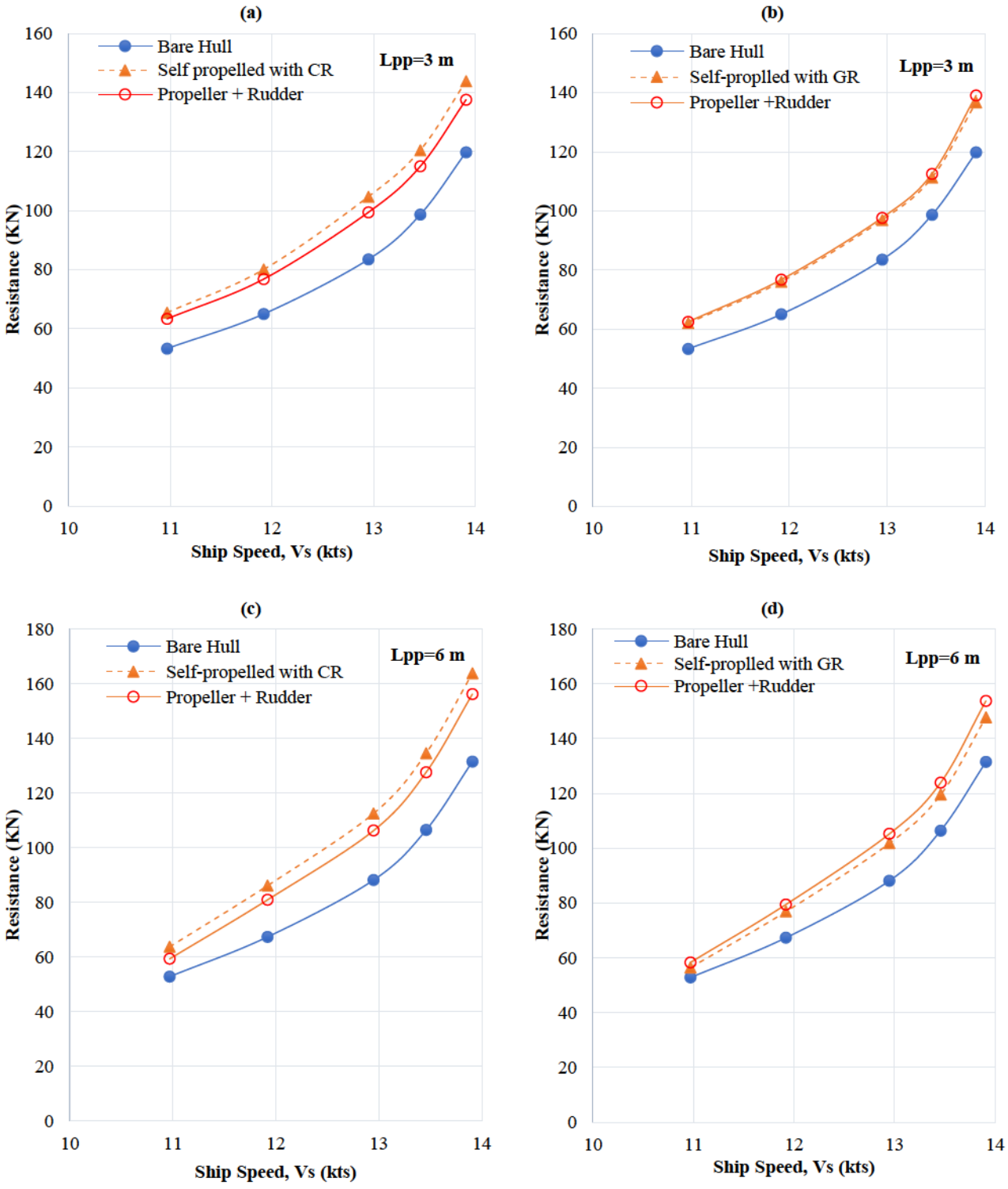

Fig. 10 Ship resisatnce predicted by 3 m and 6 m models

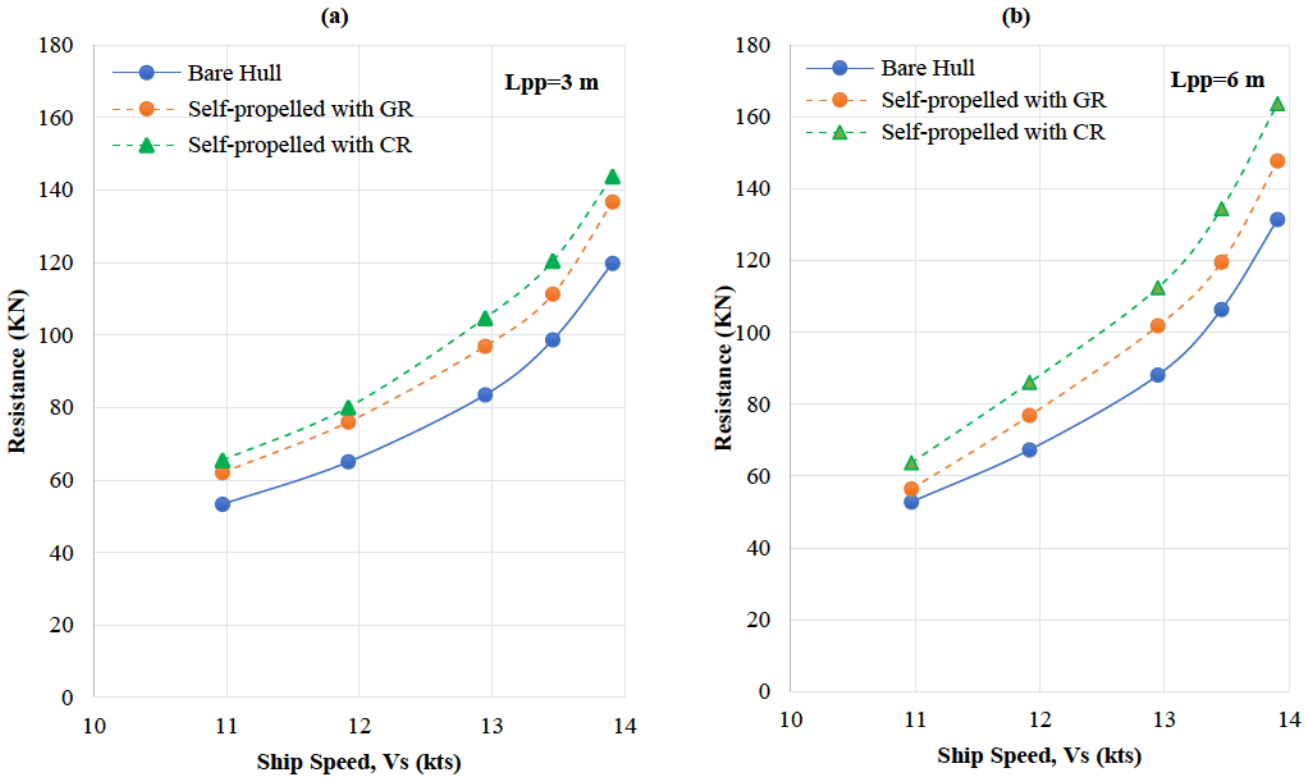

Fig. 11 Scale Effects of Ship Resistance with Conventional and Gate Rudder

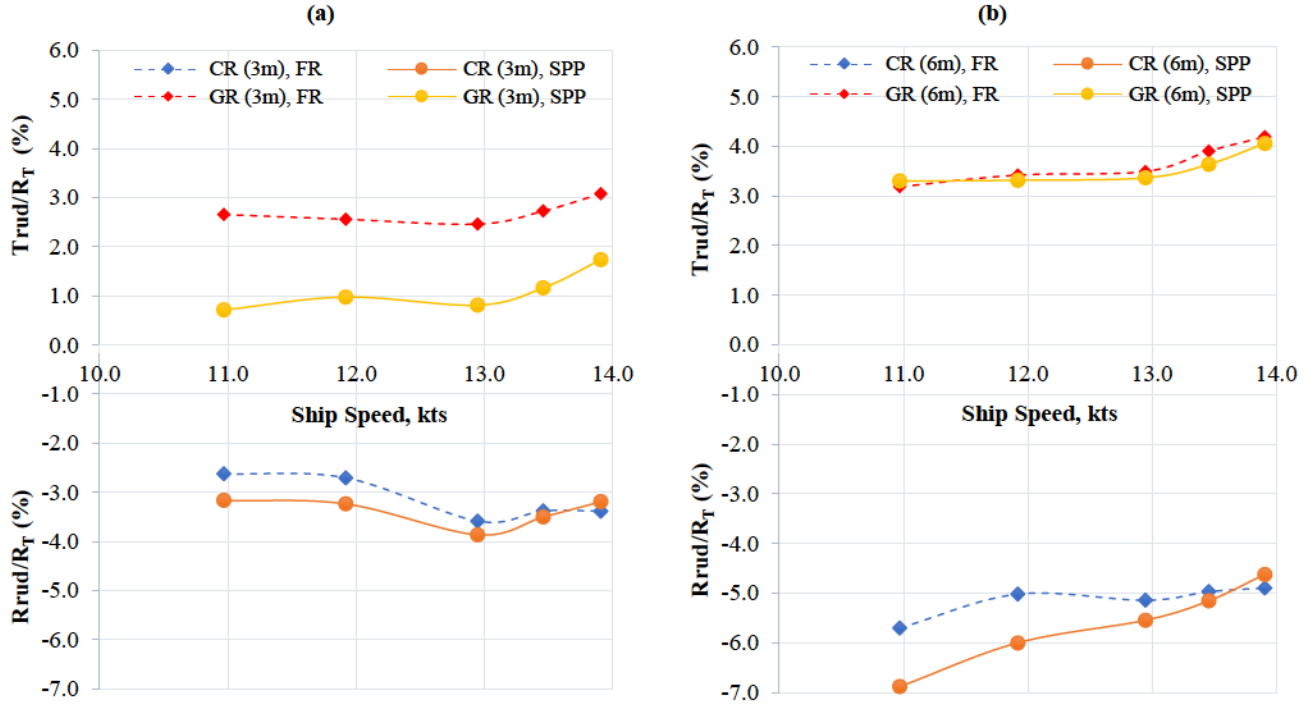

Fig. 12 Scale effects of rudder resistance of conventional rudder and thrust of gate rudder at full load condition (a) 3 m model (b) 6 m model

Fig. 12 shows the scale effects of conventional rudder resistance and gate rudder thrust generation with respect to total ship resistance obtained in self-propulsion simulations, where FR represents the free running self-propulsion simulations (i.e., SFC=0) and SPP represent the ship self-propulsion point (i.e., $T = R_T$ (SP) –SFC). It is seen from Fig. 10, the ratio of the thrust generation (negative resistance) by gate rudder to the total ship resistance around the service speed is 1.031% higher for 6 m model compared to 3 m model in model self-propulsion point (SFC=0) and about 2.55% higher at ship self-propulsion point. It is very clear from Fig. 10 that the conventional rudder gives higher resistance for 6 m compared to 3 m model and on the other hand gate rudder with 6m model gives higher thrust compared to 3 m model in both model and ship self-propulsion point. Fig. 13 shows the dynamic pressure distribution on rudder surface of conventional and gate rudder for two different scales. Larger pressure recoveries have been observed with larger model in both type of rudders. In comparison of pressure recovery between the conventional and gate rudder, more dynamic pressure distribution at the conventional rudder is appeared. That means gate rudder produces lower pressure because of high velocity at the inside of rudder blades and which generates the forward thrust.

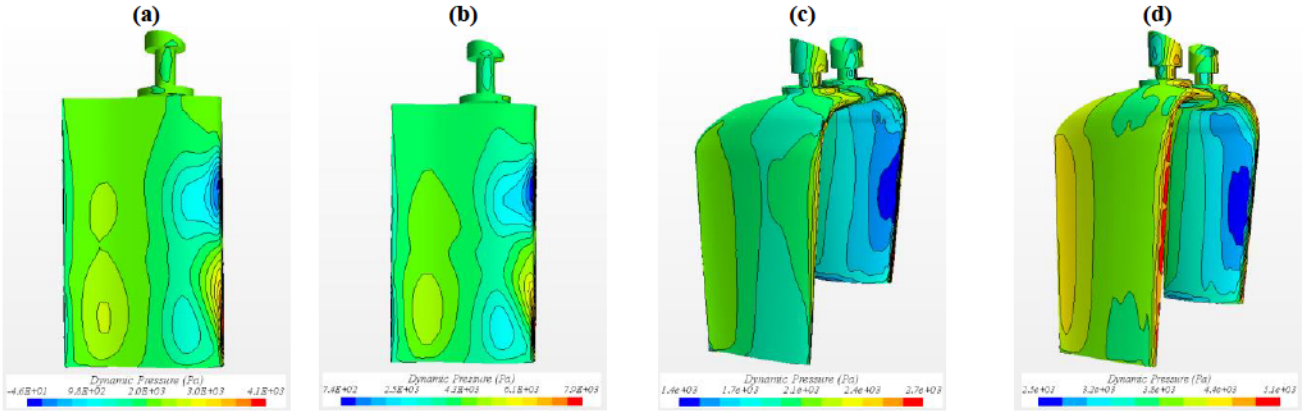

Fig. 13 Dynamic pressure distribution on rudder; Self-propelled hull in full load condition at Fr No 0.256; (a) Conventional rudder, 3 m model (b) Conventional rudder, 6 m model (c) Gate rudder, 3 m model (d) Gate rudder, 6 m model

Table 10 Summary of resistance and powering calculations predicted by 3 m Hull with Conventional Rudder by CFD, Sea trial condition at ship propulsion point

(a) Towing simulations

Vm(m/s)	Froude No	Rem	$C_{TM} \times 10^{-3}$ (Bare Hull)	R_{TM} (N) (Hull with CR)	$C_{TM} \times 10^{-3}$ (Hull with CR)	$C_{FM} \times 10^{-3}$ (Hull With CR)	$C_{PM} \times 10^{-3}$ (Hull With CR)
1.233	0.224	3.25E+06	4.031	5.175	4.057	3.189	0.868
1.394	0.253	3.67E+06	4.156	6.790	4.165	3.163	1.002
1.502	0.273	3.96E+06	4.468	8.503	4.498	3.081	1.417

(b) Self-propulsion simulation at ship propulsion point

Froude No	R_{TM} (N)	$C_{TM} \times 10^{-3}$	$C_{FM} \times 10^{-3}$	$C_{FM} \times 10^{-3}$ (ITTC)	SFC (N)	Rrud (N)	n (rps)	T (N)	Q (N-m)	K_T	K_Q
0.224	5.832	4.571	3.234	3.663	2.372	0.140	16.43	4.055	0.053	0.125	0.016
0.253	7.839	4.808	3.237	3.578	2.906	0.256	18.36	4.803	0.064	0.119	0.015
0.273	10.019	5.299	3.196	3.529	3.286	0.276	20.21	5.816	0.078	0.119	0.015

(c) Resistance extrapolation to full scale

Froude No	Vm (m/s)	Vs (m/s)	Rem	Res	$C_{FS} \times 10^{-3}$	$C_{RM} \times 10^{-3} = C_{RS} \times 10^{-3}$	ΔC_F	$C_{TS} \times 10^{-3}$	R_T (kN)
0.224	1.233	5.916	3.25E+06	3.50E+08	1.751	0.690	0.713	3.505	53.76
0.253	1.394	6.687	3.67E+06	3.95E+08	1.723	0.924	0.713	3.705	72.2
0.273	1.502	7.205	3.96E+06	4.26E+08	1.707	1.464	0.713	4.225	96.81

(d) Propulsive factors, powering and fuel oil consumption calculation

Froude No	Vs (m/s)	t	w	η_H	η_o	η_R	η	P_E (kW)	P_D (kW)	P_B (kW)	FOC (ton/day)
0.224	5.916	0.170	0.390	1.361	0.475	0.981	0.628	318.0	507.8	523.5	2.51
0.253	6.687	0.221	0.376	1.249	0.514	0.988	0.634	486.9	767.7	791.4	3.80
0.273	7.205	0.270	0.380	1.177	0.543	1.014	0.648	697.5	1086.2	1119.8	5.38

Table 11 Summary of resistance and powering calculations predicted by 3 m Hull with Gate Rudder by CFD, Sea trial condition at ship propulsion point

(a) Towing simulations

Vm(m/s)	Froude No	Rem	$C_{TM} \times 10^{-3}$ (Bare Hull)	R_{TM} (N) (Hull with GR)	$C_{TM} \times 10^{-3}$ (Hull with GR)	$C_{FM} \times 10^{-3}$ (Hull With GR)	$C_{PM} \times 10^{-3}$ (Hull With GR)
1.233	0.224	3.25E+06	4.031	5.674	4.448	3.486	0.962
1.394	0.253	3.67E+06	4.156	7.295	4.475	3.360	1.115
1.502	0.273	3.96E+06	4.468	9.424	4.984	3.311	1.673

(b) Self-propulsion simulation at ship propulsion point

Froude No	R_{TM} (N)	$C_{TM} \times 10^{-3}$	$C_{FM} \times 10^{-3}$	$C_{FM} \times 10^{-3}$ (ITTC)	SFC (N)	Trud (N)	n (rps)	T (N)	Q (N-m)	K_T	K_Q
0.224	6.050	4.767	3.502	3.684	2.372	0.053	14.10	3.625	0.072	0.153	0.021
0.253	7.820	4.951	3.372	3.599	2.906	0.067	16.40	4.847	0.085	0.173	0.020
0.273	10.314	5.455	3.374	3.549	3.286	0.101	17.60	6.927	0.096	0.215	0.019

(c) Resistance extrapolation to full scale

Froude No	Vm (m/s)	Vs (m/s)	Rem	Res	$C_{FS} \times 10^{-3}$	$C_{RM} \times 10^{-3} = C_{RS} \times 10^{-3}$	ΔC_F	$C_{TS} \times 10^{-3}$	R_T (kN)
0.224	1.233	5.916	3.25E+06	3.50E+08	1.751	0.321	0.713	3.136	51.2
0.253	1.394	6.687	3.67E+06	3.95E+08	1.723	0.478	0.713	3.259	67.8
0.273	1.502	7.205	3.96E+06	4.26E+08	1.707	1.407	0.713	4.168	89.8

(d) Propulsive factors, powering, and fuel oil consumption calculation

Froude No	Vs (m/s)	t	w	η_H	η_o		η_R	η	P_E (kW)	P_D (kW)	P_B (kW)	FOC (ton/day)
0.224	5.916	0.121	0.241	1.158	0.557		0.991	0.639	302.9	476.8	491.5	2.36
0.253	6.687	0.127	0.237	1.144	0.561		1.011	0.649	453.2	700.9	722.6	3.47
0.273	7.205	0.151	0.223	1.095	0.597		0.985	0.644	647.0	988.8	1019.4	4.89

Table 12 Summary of resistance and powering calculations predicted by 6 m Hull with Conventional Rudder by CFD, Sea trial condition at ship propulsion point

(a) Towing simulations

Froude No	Vm(m/s)	Rem	$C_{TM} \times 10^{-3}$ (Bare Hull)	R_{TM} (N) (Hull with CR)	$C_{TM} \times 10^{-3}$ (Hull with CR)	$C_{FM} \times 10^{-3}$ (Hull With CR)	$C_{PM} \times 10^{-3}$ (Hull With CR)
0.224	1.744	4.74E+06	3.162	33.210	3.254	2.488	0.766
0.253	1.972	5.35E+06	3.280	43.807	3.359	2.441	0.918
0.273	2.124	5.77E+06	3.743	57.699	3.815	2.433	1.382

(b) Self-propulsion simulation at ship propulsion point

Froude No	R_{TM} (N)	$C_{TM} \times 10^{-3}$	$C_{FM} \times 10^{-3}$	$C_{FM} \times 10^{-3}$ (ITTC)	SFC (N)	Rrud (N)	n (rps)	T (N)	Q (N-m)	K_T	K_Q
0.224	40.399	3.958	2.890	2.965	8.51	1.969	12.25	31.899	1.06	0.153	0.022
0.253	53.518	4.104	2.831	2.907	10.35	2.183	14.25	43.168	1.462	0.157	0.022
0.273	68.431	4.524	2.805	2.873	11.67	2.334	16.65	56.761	2.066	0.166	0.023

(c) Resistance extrapolation to full scale

Froude No	Vm (m/s)	Vs (m/s)	Rem	Res	$C_{FS}\times10^{-3}$	$C_{RM}\times10^{-3}=C_{RS}\times10^{-3}$	ΔC_F	$C_{TS}\times10^{-3}$	R_T (kN)
0.224	1.744	5.916	4.74E+06	3.50E+08	1.751	0.996	0.713	3.473	55.26
0.253	1.972	6.687	5.35E+06	3.95E+08	1.723	1.213	0.713	3.649	74.18
0.273	2.124	7.205	5.77E+06	4.26E+08	1.707	1.621	0.713	4.041	95.37

(d) Propulsive factors, powering, and fuel oil consumption calculation

Froude No	Vs (m/s)	t	w	η_H	η_o	η_R	η	P_E (kW)	P_D (kW)	P_B (kW)	FOC (ton/day)
0.224	5.916	0.225	0.381	1.252	0.487	1.040	0.634	326.9	517.3	533.3	2.33
0.253	6.687	0.224	0.405	1.304	0.491	1.010	0.647	496.0	770.0	793.8	3.42
0.273	7.205	0.189	0.403	1.358	0.497	0.997	0.674	687.2	1051.8	1084.4	4.74

Table 13 Summary of resistance and powering calculations predicted by 6 m Hull with Gate Rudder by CFD, Sea trial condition at ship propulsion point

(a) Towing simulations

Froude No	Vm(m/s)	Rem	$C_{TM}\times10^{-3}$ (Bare Hull)	R_{TM} (N) (Hull with GR)	$C_{TM}\times10^{-3}$ (Hull with GR)	$C_{FM}\times10^{-3}$ (Hull With GR)	$C_{PM}\times10^{-3}$ (Hull With GR)
0.224	1.744	4.74E+06	3.162	35.839	3.512	2.656	0.856
0.253	1.972	5.35E+06	3.280	48.805	3.742	2.612	1.131
0.273	2.124	5.77E+06	3.743	63.063	4.169	2.585	1.584

(b) Self-propulsion simulation at ship propulsion point

Froude No	R_{TM} (N)	$C_{TM}\times10^{-3}$	$C_{FM}\times10^{-3}$	$C_{FM}\times10^{-3}$ (ITTC)	SFC (N)	Trud (N)	n (rps)	T (N)	Q (N-m)	K_T	K_Q
0.224	39.423	3.863	2.691	2.965	8.38	0.697	11.74	29.820	0.992	0.157	0.019
0.253	53.685	4.116	2.562	2.907	10.41	0.826	13.50	40.935	1.323	0.150	0.020
0.273	68.739	4.545	2.563	2.873	11.81	1.020	15.20	55.464	1.422	0.132	0.018

(c) Resistance extrapolation to full scale

Froude No	Vm (m/s)	Vs (m/s)	Rem	Res	$C_{FS}\times10^{-3}$	$C_{RM}\times10^{-3}=C_{RS}\times10^{-3}$	ΔC_F	$C_{TS}\times10^{-3}$	R_T (kN)
0.224	1.744	5.916	4.74E+06	3.50E+08	1.751	0.633	0.713	3.049	48.51
0.253	1.972	6.687	5.35E+06	3.95E+08	1.723	0.785	0.713	3.221	65.49
0.273	2.124	7.205	5.77E+06	4.26E+08	1.707	1.296	0.713	3.716	87.70

(d) Propulsive factors, powering, and fuel oil consumption calculation

Froude No	Vs (m/s)	t	w	η_H	η_o	η_R	η	P_E (kW)	P_D (kW)	P_B (kW)	FOC (ton/day)
0.224	5.916	0.100	0.212	1.142	0.517	1.030	0.608	287.0	470.7	485.3	2.33
0.253	6.687	0.081	0.212	1.166	0.541	1.010	0.637	437.9	691.8	713.2	3.42
0.273	7.205	0.093	0.191	1.121	0.587	1.000	0.659	631.9	958.1	987.7	4.74

The similar CFD analysis at sea trial conditions were carried out for the model scale at three different speeds. The direct outputs from CFD simulations for model scale and extrapolated for full scale have been given in Tables 10–11. Fig. 14 shows the extrapolated total ship resistance for two model scales. Similar results of full load conditions can be observed from the figures in the sea trial loading condition. One can observe from Fig. 14, the ship fitted with gate rudder gives less resistance than that with conventional rudder. The reduction in total resistance obtained by 3 m ship is about 6–7% whereas it is about 8–9 % obtained by 6 m model.

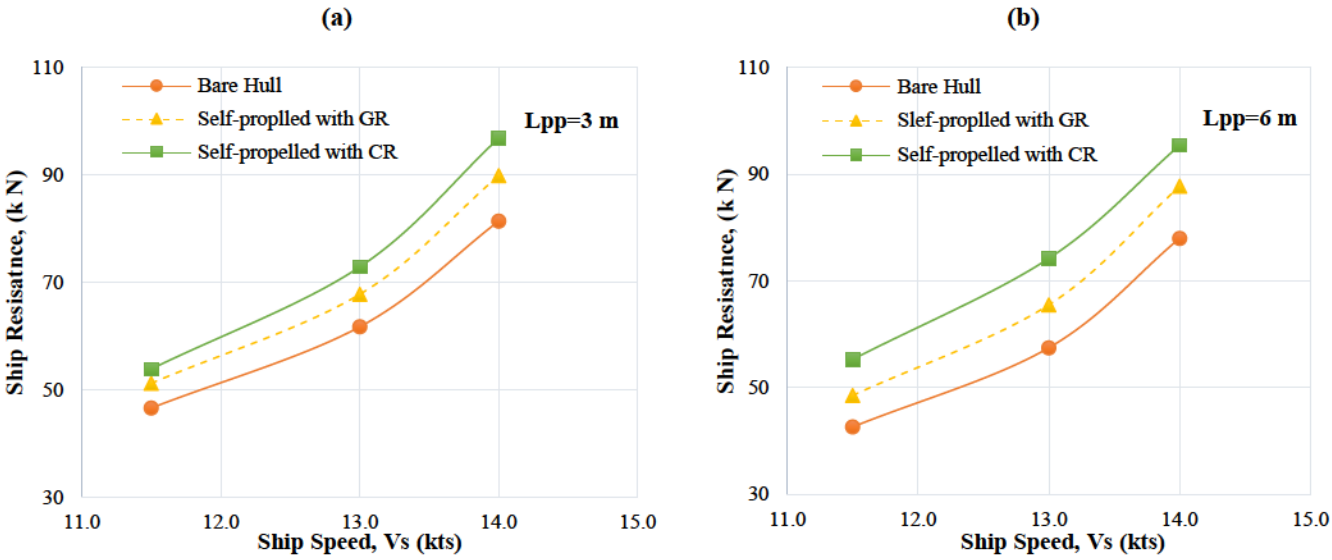

Fig. 14 Scale effects of ship resistance at sea trial loading conditions with conventional and gate rudder (a) 3 m model (b) 6 m model

The ratios of rudder resistance to total ship resistance have been plotted in Fig. 15 to demonstrates the scale effects of gate rudder performance. It is seen that the contribution of conventional rudder in total resistance is 3.2 % obtained by 3 m model whereas it is about 4.3 % obtained by 6 m model. That is the conventional rudder has the tendency to contributes more resistance in larger scale. In Fig. 15 (a), it is also seen that at lower speed the contribution of conventional rudder resistance is higher. Again the Fig. 15 (b) shows that the thrust generation by gate rudder (negative resistance) is about 0.60% for 3 m model at service speed whereas the amount increases to 1.70% for 6 m model. From this phenomenon, it is pretty clear that the gate rudder generates higher thrust at larger scale.

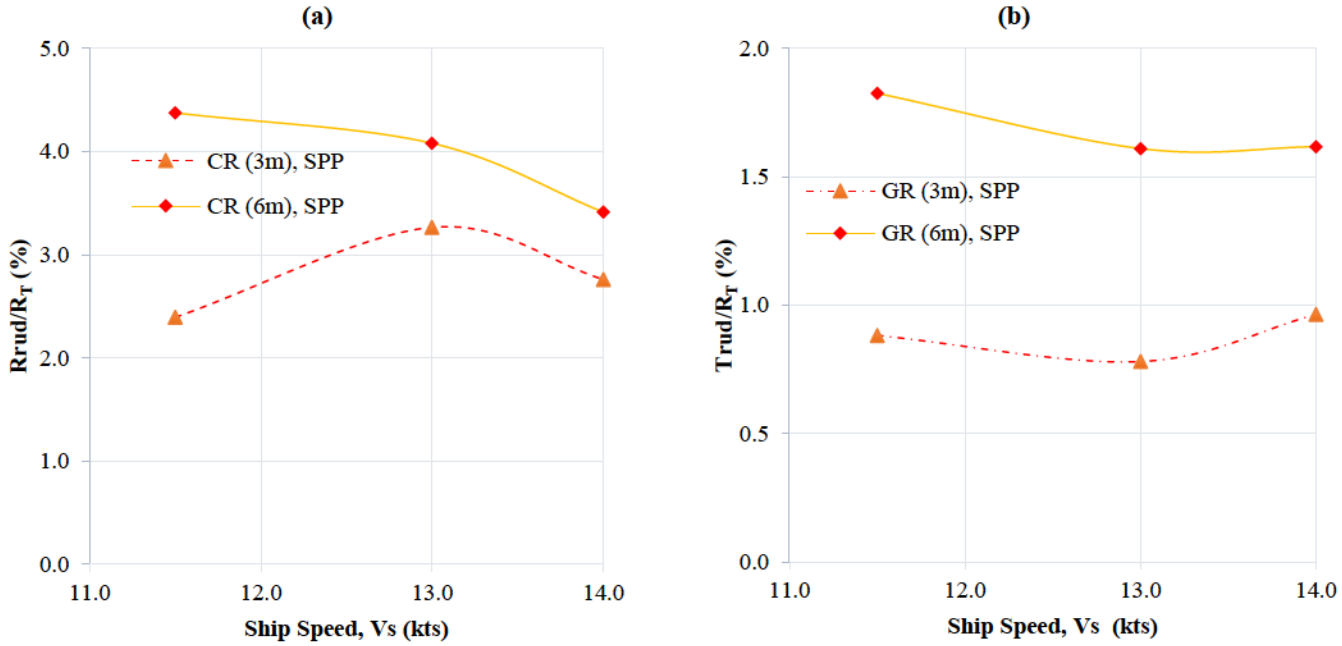

Fig. 15 Scale effects of rudder resistance and thrust at sea trial loading condition (a) Conventional rudder resistance (b) Gate rudder thrust

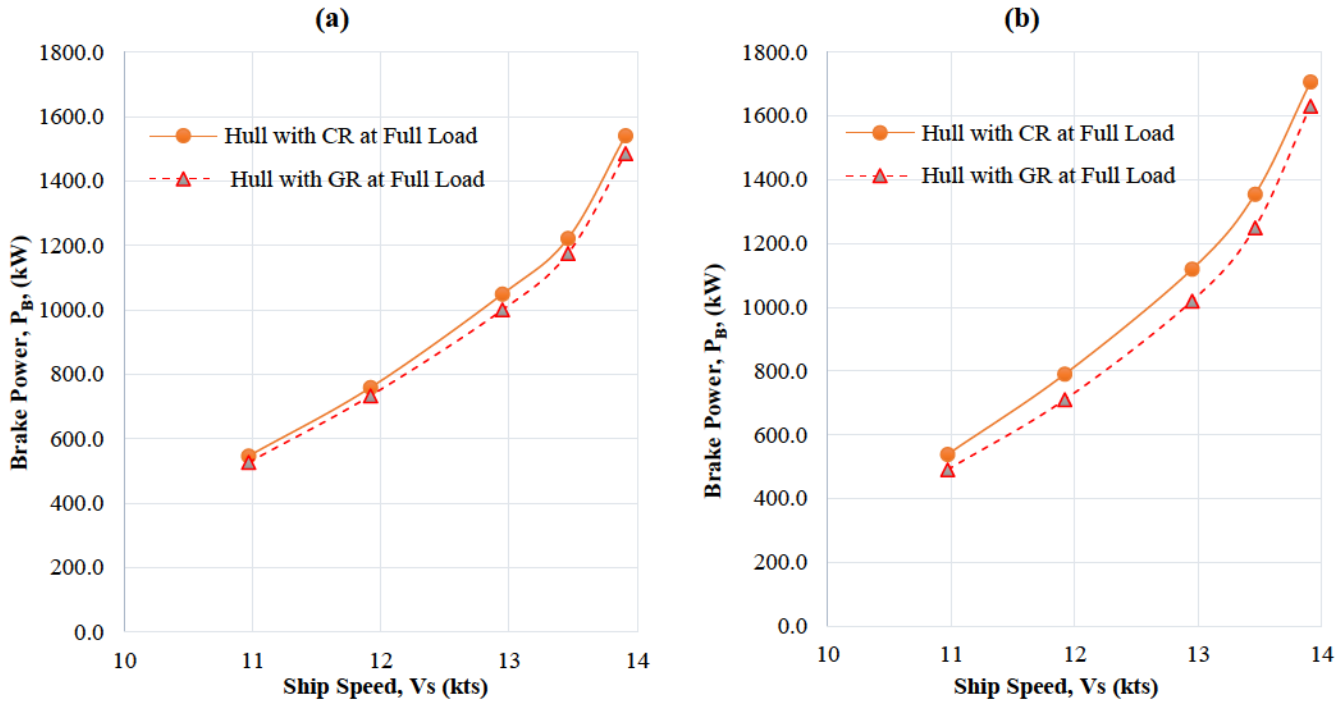

Fig. 16 Brake power requirement at full load condition predicted by (a) 3 m model and (b) 6 m model

Figs. 16 and 17 show the comparisons of brake power requirement with conventional rudder and gate rudder estimated by two different models at full load condition and sea trial condition respectively. From Figs. 16 (a) and 16 (b), it is seen that the reduction in brake power requirements is larger for 6 m model compared to 3 m model. The reduction in brake power at service speed is about 6.0–7.0 % predicted by 3 m model, whereas it is about 9–10% predicted by 6 m model at full load condition. Similar variation in brake power reduction between two models at sea trial condition is observed from Figs. 17 (a) and 17 (b).

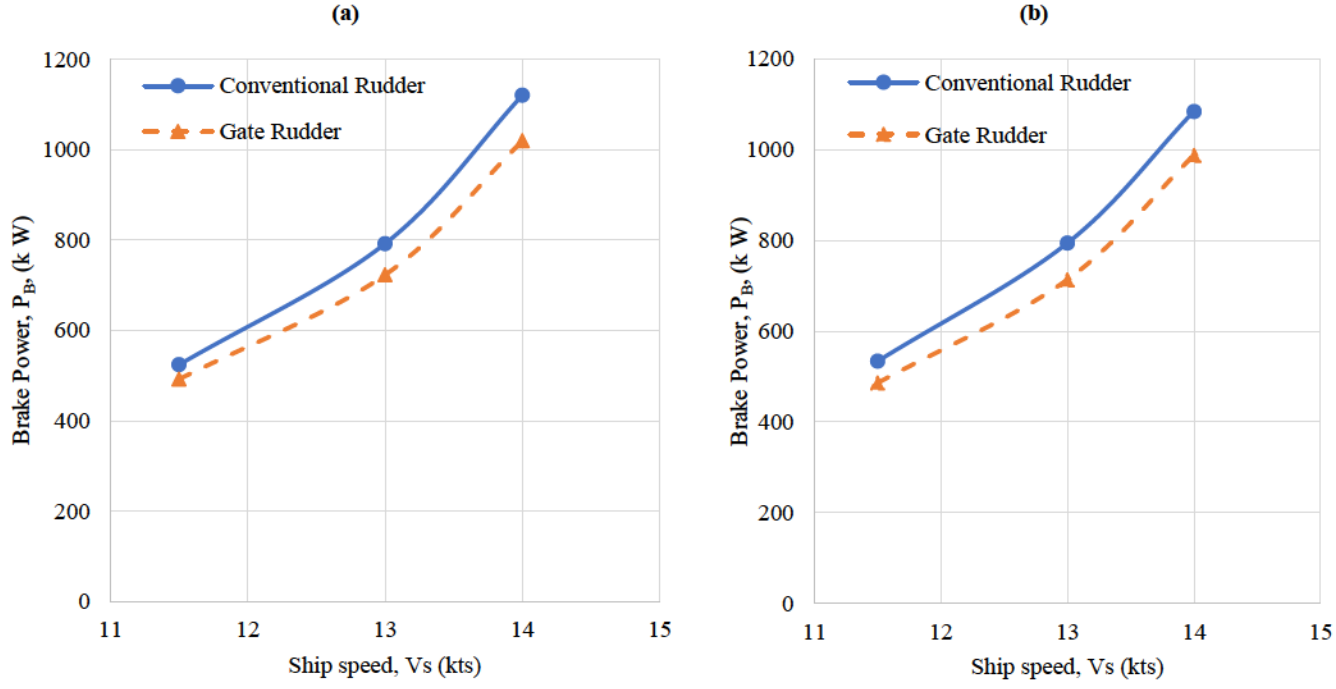

Fig. 17 Brake power requirement at sea trial condition predicted by (a) 3 m model and (b) 6 m model

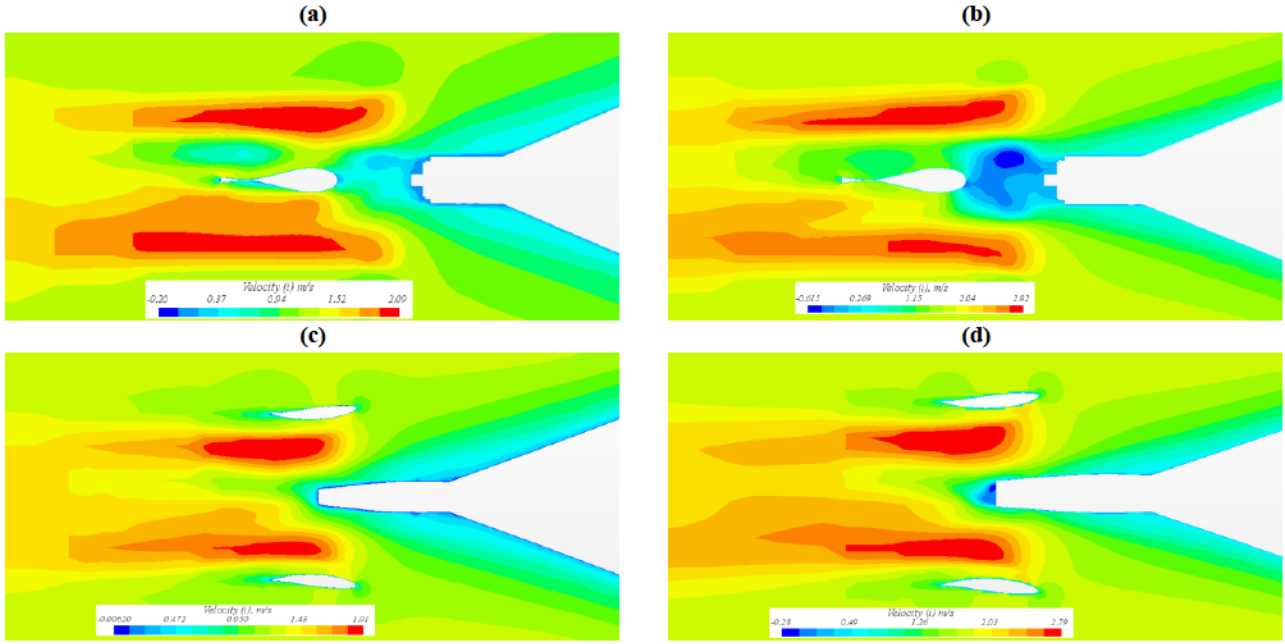

Fig. 18 Axial Velocity contour at top plane along shaft axis; Self-propelled hull in full load condition at Fr No 0.256; (a) Conventional rudder of 3 m model (b) Conventional rudder of 6 m model (c) Gate rudder of 3 m model (d) Gate rudder of 6 m model

The axial velocity flow contours have been shown in Fig. 18 for Froude No. 0.256 from which at the propeller plane with gate rudder has higher inflow velocity compared to conventional rudder. Again, propeller fitted with gate rudder to 6 m hull receives higher inflow velocity at the propeller plane than that of 3 m model.

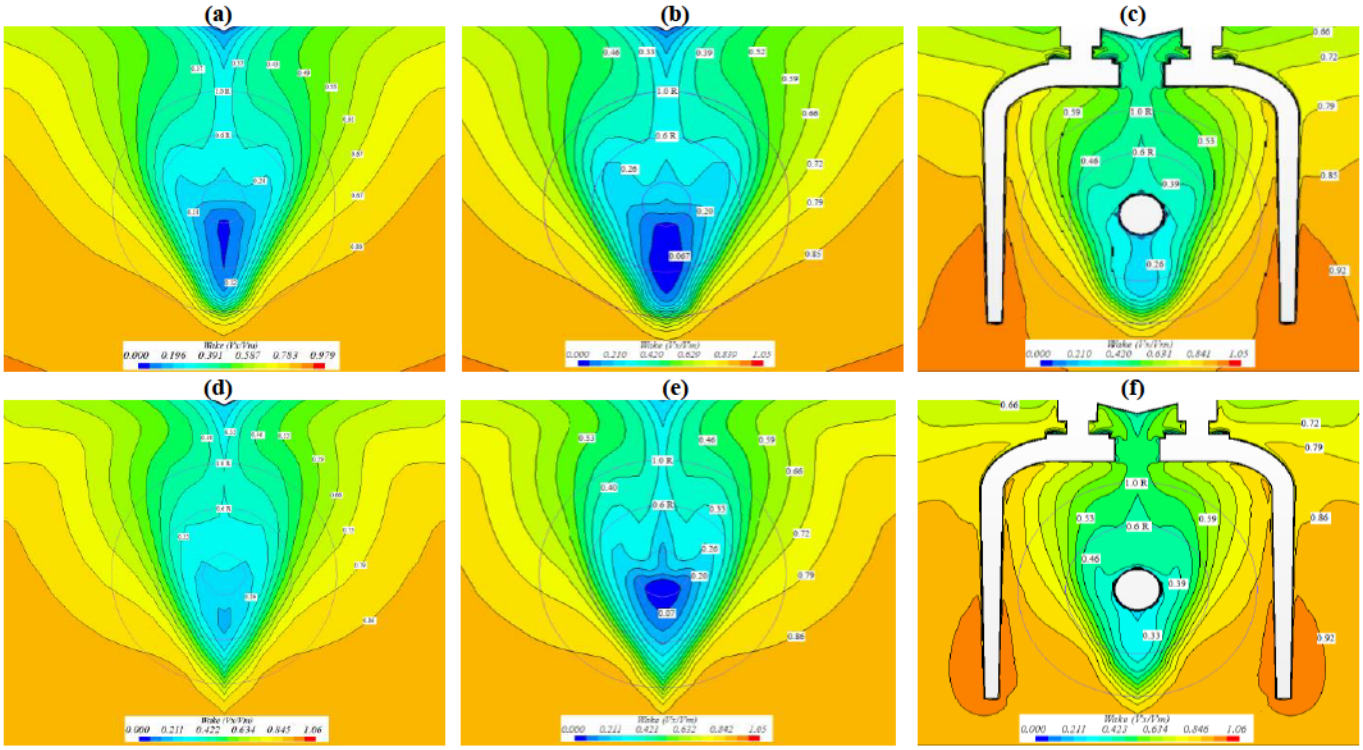

Fig. 19 Wake Field at propeller plane in towing condition; Full Load Condition at Fr No 0.256 (a) 3 m model with bare hull (b) 3 m model with conventional rudder (c) 3 m model with gate rudder (d) 6 m model with bare hull (e) 6 m model with conventional rudder (f) 6 m model with gate rudder

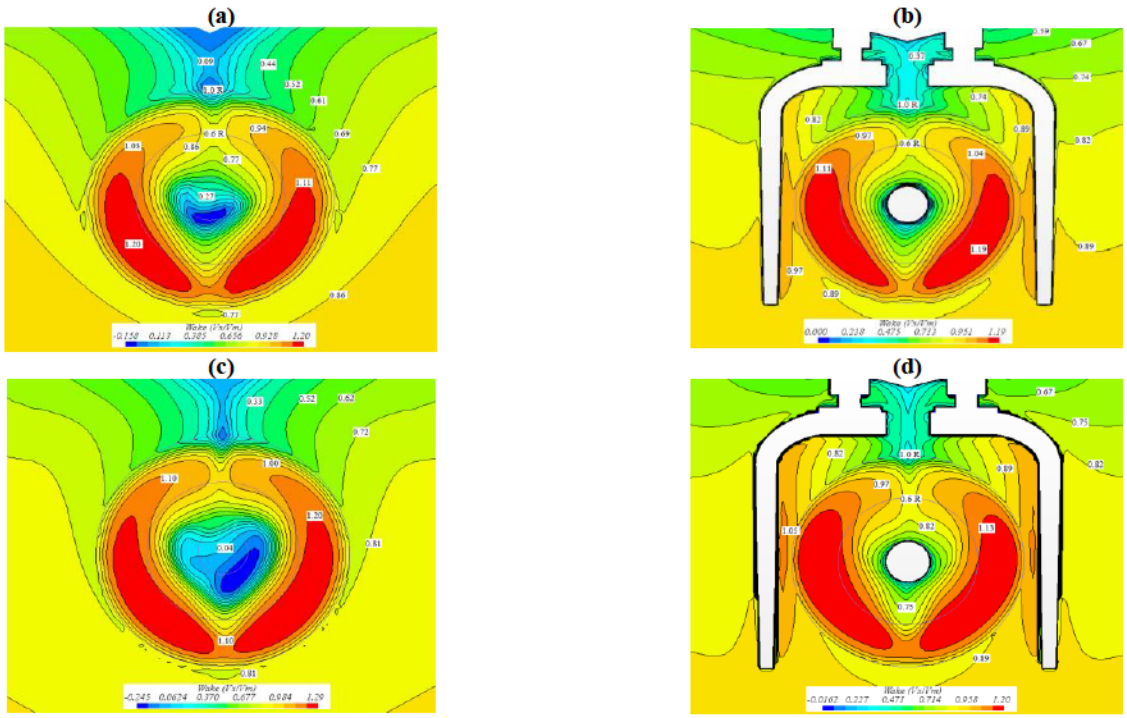

Fig. 20 Wake Field at propeller plane in self-propelled condition; Full Load Condition at Fr No. 0.256 (a) 3 m model with conventional rudder (b) 3 m model with gate rudder (c) 6 m model with conventional rudder (d) 6 m model with gate rudder

The wake field at the propeller plane is depicted in Fig. 19 for the model at towing without rudder, with conventional rudder and with gate rudder for 3 m and 6 m models respectively in full load condition. The wake field presented here are non-dimensionalized by dividing the axial velocity with model velocity. The wake field can be divided in two different zones: the flow within the propeller disk area and the flow outside the propeller disk. The flow inside the propeller is showing an asymmetric configuration. The wake filed at the propeller plane in self-propelled condition has been shown in Fig. 20 and the circumferential wake distraction at 0.7 R for both model scales have been shown in Fig. 21.

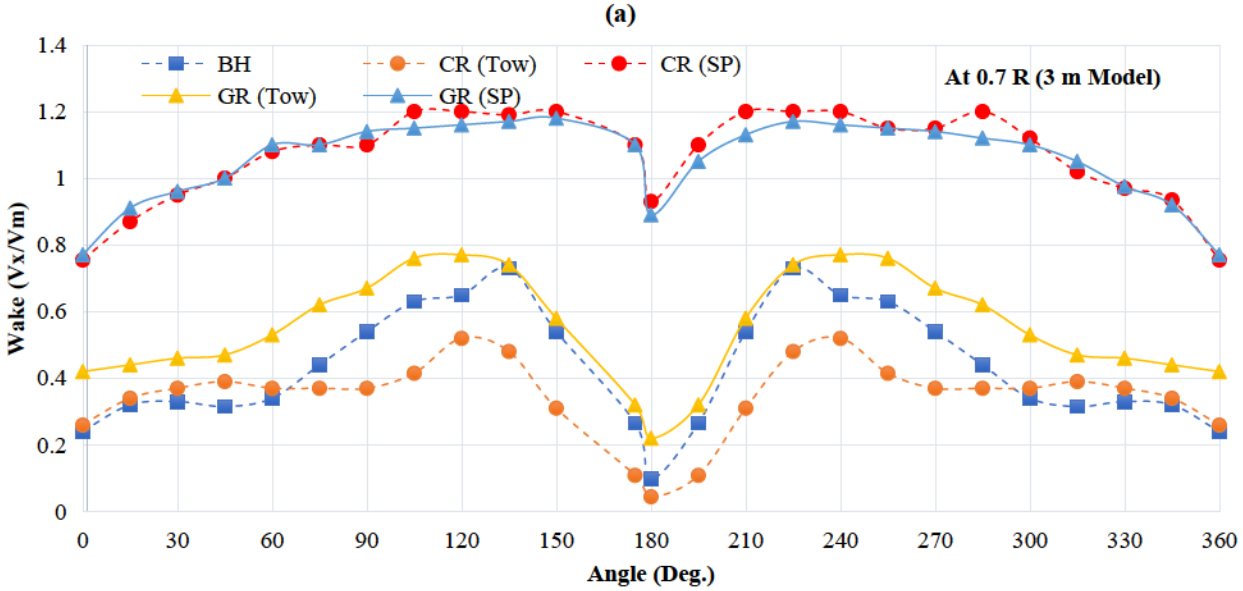

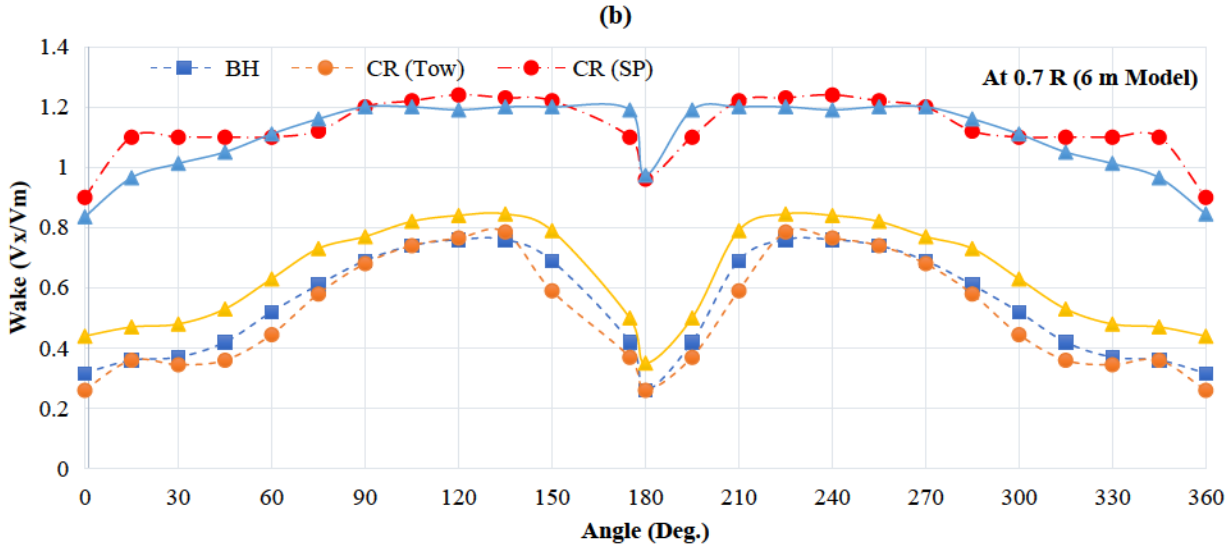

Fig. 21 Circumferential Wake (Vx/Vm) distribution at 0.7 R of the propeller disk; Self-propelled hull in full load condition at Fr No 0.256 with (a) 3m model and (b) 6 m model

Though a number of evidence shows the reliability and accuracy of the predicted hull performance parameters and design of energy saving device based on the Computational Fluid Dynamics (CFD) at model scale, it may often have a discrepancy with the full-scale ship performance. Wake field behind the hull of a model always varies with the hull of a ship due to different flow characteristics at high Reynolds Number. With the improvement of numerical simulation tools and advancement of computational power, the full scale CFD analysis provides more accurate prediction of hull–propeller interaction with energy saving devices and eliminates the need of complex extrapolation procedure. CFD analyses of the ship at full scale have been carried out for three different speeds at full load conditions. The numerical results have been verified and validated following ITTC recommendation which have been presented in Section 3. Tables 14–15 represent the summary of the full-scale simulation results and calculations.

Table 14 Summary of resistance and powering calculations predicted by full scale ship with Conventional Rudder by CFD, full load condition at ship propulsion point

(e) Towing simulations

Froude No	Vs (m/s)	$C_T \times 10^{-3}$ (Bare Hull)	R_T (kN) (Hull with CR)	$C_T \times 10^{-3}$ (Hull with CR)	$C_F \times 10^{-3}$ (Hull With CR)	$C_P \times 10^{-3}$ (Hull With CR)	$C_F \times 10^{-3}$ (ITTC)
0.2265	6.132	3.267	72.74	3.326	1.828	1.497	1.748
0.2461	6.661	3.337	86.94	3.369	1.783	1.586	1.729
0.2644	7.155	3.567	107.65	3.615	1.756	1.859	1.712

(f) Self-propulsion simulation at ship propulsion point

Froude No	R_T (kN)	$C_T \times 10^{-3}$	$C_F \times 10^{-3}$	Rrud (kN)	N (rps)	J	T (kN)	Q (kN-m)	K_T	K_Q
0.2265	89.75	4.104	1.860	3.034	4.5	0.42	91.23	28.174	0.132	0.017
0.2461	108.72	4.213	1.816	3.718	4.8	0.42	108.88	29.079	0.139	0.015
0.2644	131.67	4.422	1.803	4.549	5.4	0.41	128. 5	36.876	0.132	0.015

(g) Propulsive factors and powering calculation

Froude No	Vs (m/s)	Va (m/s)	t	w	η_H	η_o	η_R	η	P_E (kW)	P_B (kW)
0.2265	6.132	4.536	0.190	0.260	1.096	0.562	0.968	0.596	550	910
0.2461	6.661	4.838	0.200	0.274	1.101	0.569	1.035	0.648	724	1127
0.2644	7.155	5.314	0.182	0.257	1.101	0.562	1.033	0.639	942	1520

Table 15 Summary of resistance and powering calculations predicted by full scale ship with Gate Rudder by CFD, full load condition at ship propulsion point

(a) Towing simulations

Froude No	Vs (m/s)	$C_T \times 10^{-3}$ (Bare Hull)	R_T (kN) (Hull with GR)	$C_T \times 10^{-3}$ (Hull with GR)	$C_F \times 10^{-3}$ (Hull With GR)	$C_P \times 10^{-3}$ (Hull With GR)	$C_F \times 10^{-3}$ (ITTC)
0.2265	6.132	3.267	73.91	3.326	1.790	1.537	1.748
0.2461	6.661	3.337	88.77	3.386	1.753	1.633	1.729
0.2644	7.155	3.567	108.95	3.602	1.752	1.850	1.712

(b) Self-propulsion simulation at ship propulsion point

Froude No	R_T (kN)	$C_T \times 10^{-3}$	$C_F \times 10^{-3}$	Rrud (kN)	N (rps)	J	T (kN)	Q (kN-m)	K_T	K_Q
0.2265	82.06	3.693	1.795	4941	3.95	0.53	82.06	30.05	0.155	0.024
0.2461	98.67	3.763	1.803	6254	4.38	0.53	98.67	33.35	0.151	0.021
0.2644	119.47	3.949	1.765	6361	4.66	0.53	119.47	43.58	0.162	0.025

(c) Propulsive factors and powering calculation

Froude No	Vs (m/s)	Va (m/s)	t	w	η_H	η_o	η_R	η	P_E (kW)	P_B (kW)
0.2265	6.132	5.024	0.099	0.181	1.099	0.619	0.953	0.649	503	800
0.2461	6.661	5.571	0.100	0.164	1.076	0.619	1.038	0.691	657	981
0.2644	7.155	5.928	0.088	0.172	1.101	0.619	0.976	0.665	855	1325

The obtained resistance coefficients have been presented in Fig. 22. In Fig. 22 (a), the total resistance coefficients and friction resistance coefficients at towing and self-propelled condition of the ship with conventional rudder and in Fig. 22 (b), the coefficients for ship with gate rudder are presented. In both cases, the predicted frictional resistance coefficients have a good agreement with the ITTC 1957 friction line.

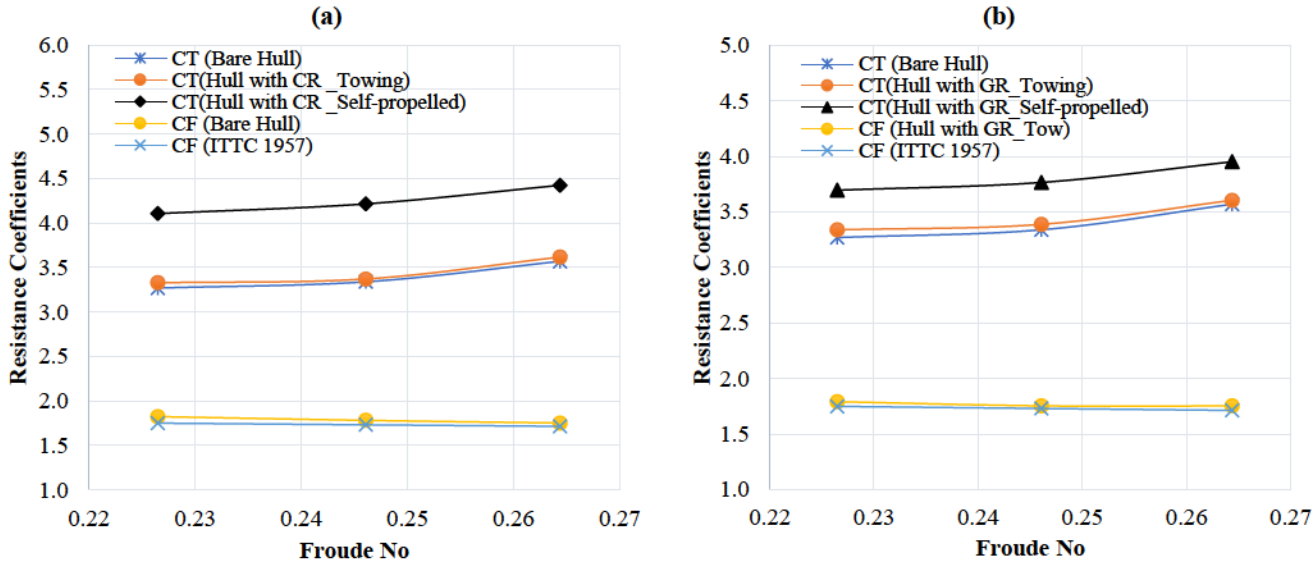

Fig. 22 Full scale ship resistance coefficients predicted by CFD (a) Conventional Rudder (b) Gate Rudder

Total resistance obtained by full scale simulations has been presented in Fig. 23(a), which shows that the ship with conventional rudder gives more ship resistance than that of ship with gate rudder. Total resistance of the full-scale ship has a good consistency with the extrapolated total resistance obtained by model scales at ship speed of 6.132 m/s and 6.661 m/s, although there is a certain amount of deviation at ship speed of 7.155 m/s. Fig. 23(b) shows the amount of contribution of conventional rudder resistance and gate rudder thrust in total ship resistance. In Fig. 12, it has been shown earlier that the conventional rudder contributes about 2% and 3% of total ship resistance predicted by 3 m model and 6 m model respectively at ship prolusion

point in full load conditions. In case of full-scale ship, the contribution of rudder resistance increases which is about more than 4% as shown in Fig 23(b). Again, the gate rudder produces more than 6 % thrust of total resistance obtained by full scale simulations which was about 1-2 % and about 2-3 % in case of 3m and 6m model respectively. That is ultimately more than 10 % reduction of total ship resistance. The thrust deduction factors are quite similar with the extrapolated values obtained by the model scales and full scale. The effective wake ranges about 0.21–0.24 for model scales whereas the value obtained by full scale is about 0.17–0.18.

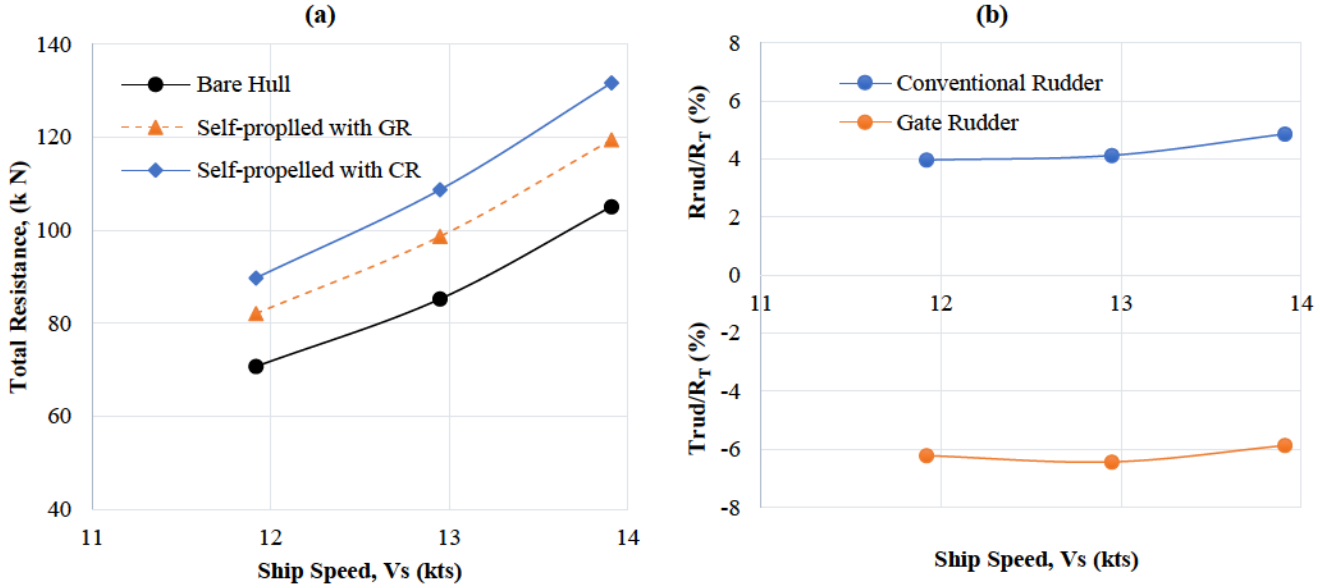

Fig. 23 Full scale CFD prediction (a) Total resistance (b) Conventional rudder resistance and gate rudder thrust to total ship resistance ratio

The propulsive factors obtained by full scale ship with conventional rudder and gate rudder have been presented in table 14–15. Improved propulsive performance has been observed with the ship with gate rudder compared to gate rudder. The Fig. 24(a) shows effective power and Fig. 24(b) brake power requirement obtained by full scale ship CFD. From Fig. 24(b), it is seen that more that 12% reduction in brake power is achieved with gate rudder system of a ship. The distribution of dynamic pressure on hull and rudders, axial velocity at the top plane along the shaft axis and wake field at the propeller plane for both cases of rudder arrangements at Froude Number 0.2664 have been shown in Fig. 26, Fig. 27, and Fig. 28 respectively.

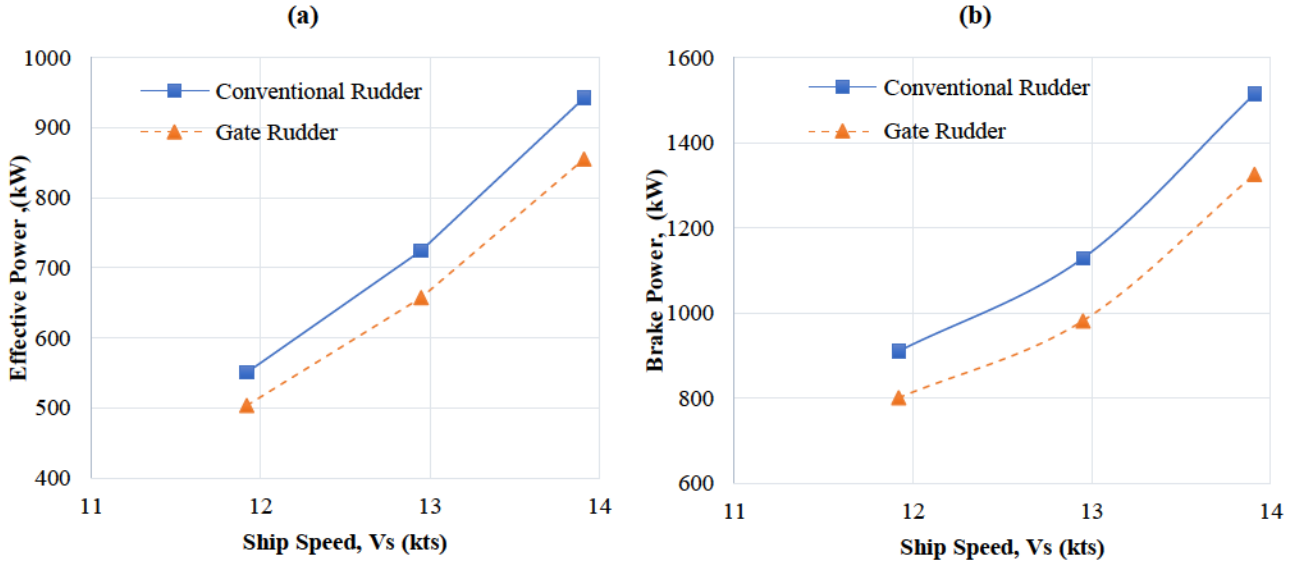

Fig. 24 Power prediction by full scale ship CFD analysis (a) Effective power (b) Brake power

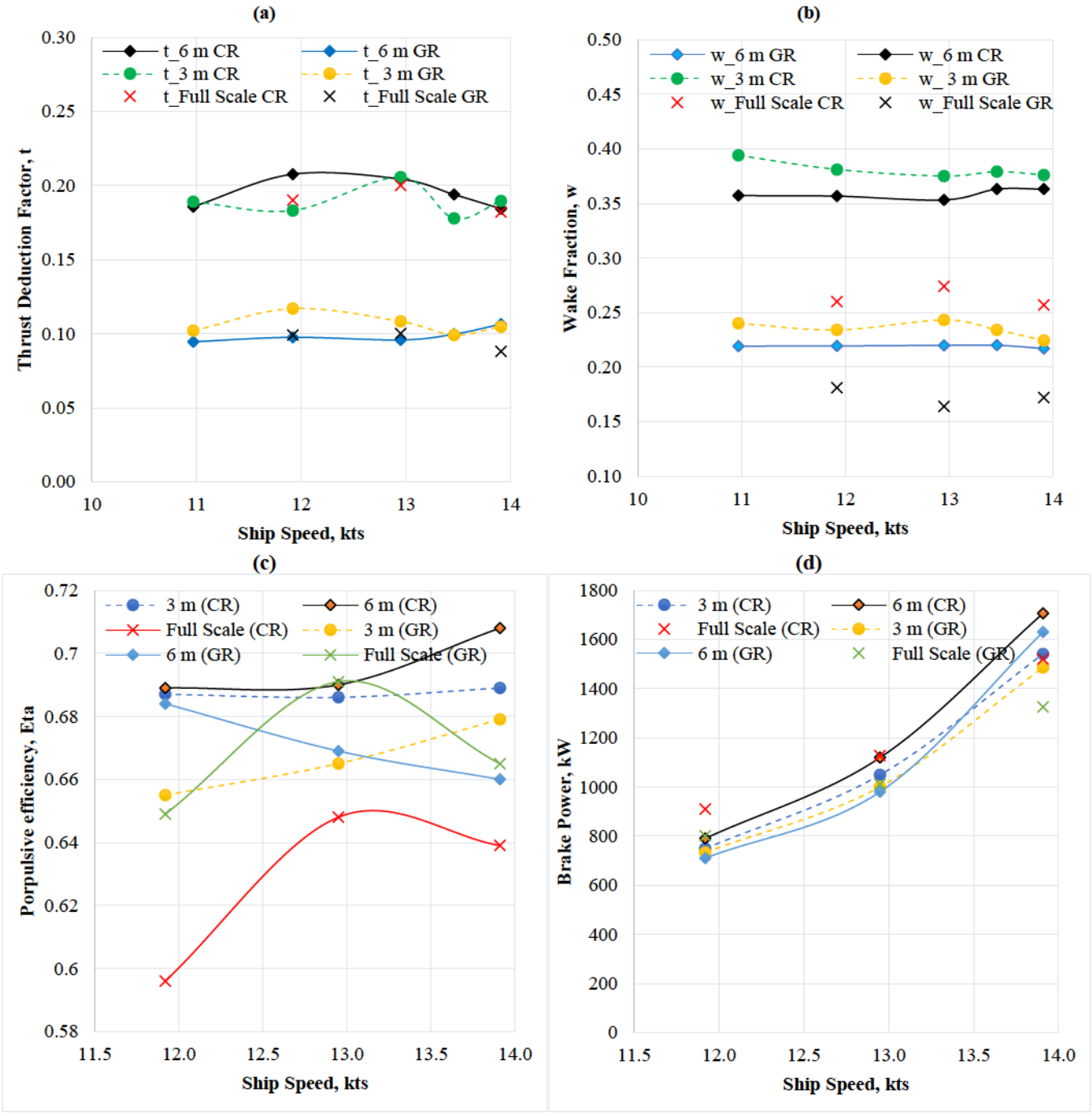

Fig. 25 Scale effects on propulsive efficiency and brake power in full load conditions (a)Thrust deduction factors (b) Wake fractions (c) Propulsive efficiency (d) Brake power

Fig. 25 depicts a clear picture of the scale effect on gate rudder performance as it summarizes self-propulsive coefficients such as thrust deduction, wake fraction, propulsive efficiency, and brake power obtained by three different scales. There is a very little effect on the thrust deduction factors. However, as shown in Fig. 25(b), the scales have a significant effect on wake fractions in both types of rudder cases. The overall propulsive efficiency varies among three scales, but the improved efficiencies are observed for a particular scale for the gate rudder system compared to conventional rudder. The improvement certainly increases on a larger scale. The extrapolated results of 3 m and 6 m are found to be in consistent and they are also consistent with the full scale at the speeds of 11.92 kts and 12.95 kts, where the deviation ranges from 4 to 8% for both cases

of the rudder at full load. However, there is a bigger difference at 13.91 kts, as shown in Fig. 25(d). There might be certain errors in the extrapolation procedure and considerations of roughness factor allowance as well. Therefore, it requires more detailed investigations in full-scale simulations to address the issue at higher speeds. However, the most important fact is that the amount of reduction in brake power is significantly higher on larger scales.

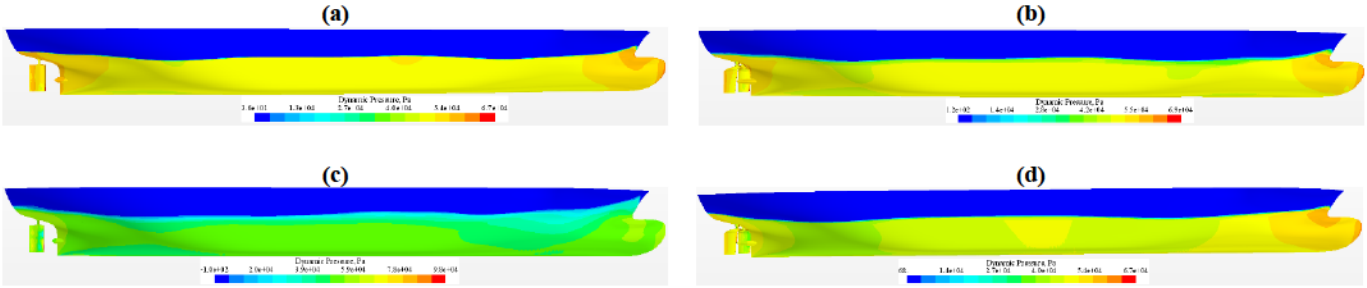

Fig. 26 Dynamic pressure distribution on the full-scale ship hull at Fr No 0.2664 (a) Conventional rudder towing condition (b) Gate rudder towing condition (c) Conventional rudder self-propulsion condition (d) Gate rudder self-propelled condition

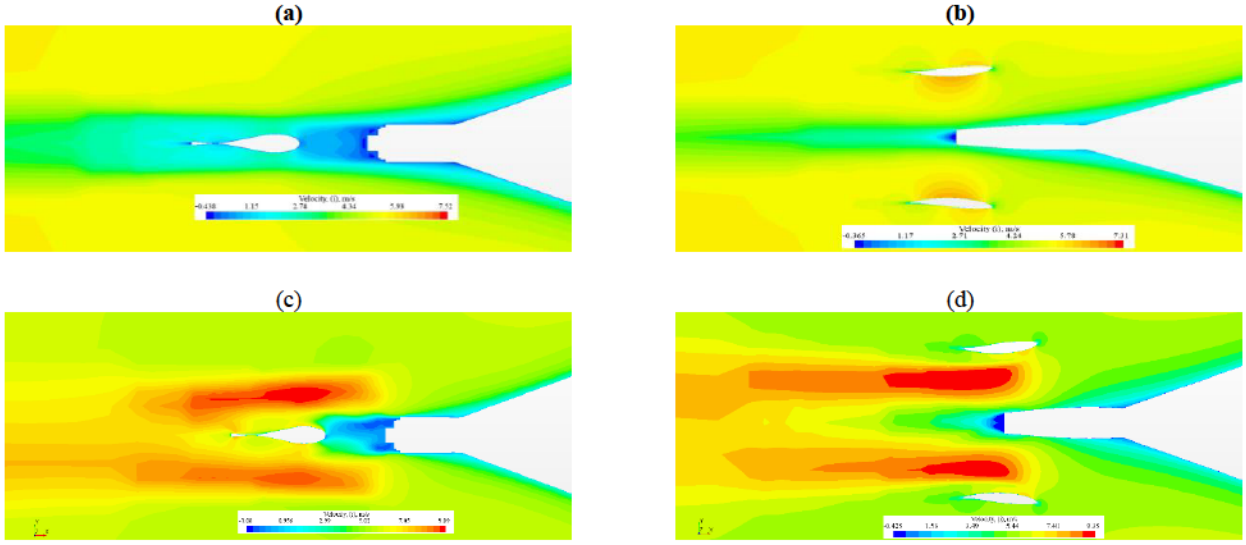

Fig. 27 Axial velocity flow distribution at aft part of the full-scale ship hull at Fr No 0.2664 (a) Conventional rudder towing condition (b) Gate rudder towing condition (c) Conventional rudder self-propulsion condition (d) Gate rudder self-propelled condition

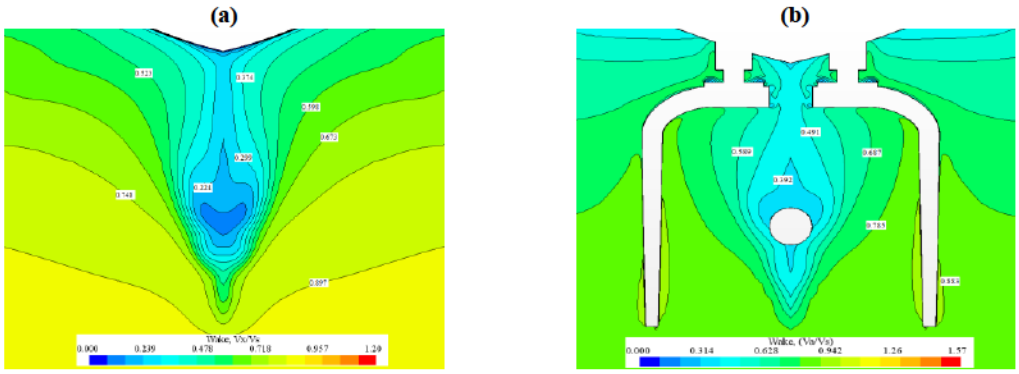

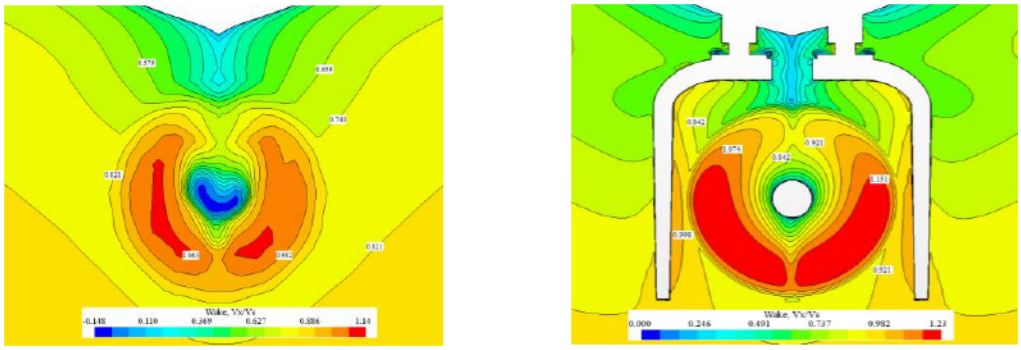

Fig. 28 Wake field distribution in the propeller plane at Fr No 0.2664 (a) Ship with conventional rudder in towing (top) and self propulsion (bottom) (b) Ship with gate rudder in towing (top) and self-propulsion (bottom)

6 Conclusion

This study numerically investigates scale effects on the propulsive performances of a domestic cargo ship fitted with a gate rudder system and a conventional rudder. The numerical analysis was carried out considering three different scales, i.e., 3 m model, 6 m model, and 69 m full-scale ship at various speeds. The model scale analyses were done for two loading conditions, i.e., full loading condition and sea trial loading condition, whereas the full-scale analysis was done for only the full loading condition of the ship. Grid convergence study and V&V study have been carried out for the 6 m model with a conventional rudder and for the full-scale ship with a gate rudder. The resistance data obtained by CFD simulations of model scales have been extrapolated to full scale following the ITTC's recommended standard procedure. The resistance components and propulsive factors were derived for each scale with both loading conditions have been discussed. The scale effects on the total resistance of conventional rudder and the total thrust generation by the gate rudder have been explained in detail. Based on the above results and discussion, the following conclusions can be drawn:

1. The accuracy of the RANS based numerical simulation has been ensured by model test data and V&V study based on grid independency test of CFD simulations.
2. There is about a 7-8% reduction in power requirements in the case of the 3 m model with the gate rudder compared to the conventional rudder and about a 9–10 % reduction in power requirements for the 6 m model with full loading condition at service speed of the ship. According to full scale analysis, more than a 12% reduction in power requirements is possible in full loading conditions at service speed of the ship.
3. There is about a 5–6% reduction in power requirements in the case of the 3 m model with the gate rudder compared to the conventional rudder and about a 7–8% reduction in power requirement for the 3 m model in sea trial condition at service speed of the ship.
4. The gate rudder of the 6 m model generates higher thrust than that of the 3 m model in both loading conditions. On the other hand, the conventional rudder contributes higher resistance in the case of the 6 m model compared to 3 m model. Again, the full-scale gate rudder generates more thrust compared to the scaled model. This indicates that the gate rudder system will provide higher thrust and excellent propulsive performance at larger scale.
5. The selected ship with the gate rudder system gives improved thrust deduction factor and wake fraction compared to the ship with the conventional rudder.
6. The ITTC wake scaling procedure can't be applied in the case of the effective wake of a gate rudder as advanced velocity is accelerated by the gate rudder blades, which is significant at lower Reynolds numbers. More full-scale data and analysis with gate rudder are required to evaluate the wake scaling procedure presented in the literature.
7. Along with significant amount of power-savings, gate rudder will demonstrate significant amount of emissions reduction from ships as it is directly related to the power and fuel oil consumptions.

References:

1. IMO (2020). Fourth IMO GHG Study – Final Report. The International Maritime Organization (IMO), London, United Kingdom. IMO Technical Report No MEPC 67/INF.3
2. Mofor L, Nuttal P, Newell A (2015). Renewable energy options for ship–Technology Brief. International Renewable Energy Agency (IRENA), Abu Dhabi, United Arab Emirates. Technical Report
3. Hussain MD and Amin OM (2021). A Comprehensive Analysis of the Stability and Powering Performances of a Hard Sail–Assisted Bulk Carrier. *J. Marine. Sci. Appl*. Vol 3, pp https://doi.org/10.1007/s11804-021-00219-w
4. Hasan SMR and Karim MM (2020). Proposed inland oil tanker design in Bangladesh focusing CO2emission reduction based on revised EEDI parameters. *J. Mar. Sci. Eng.*, Vol 8, pp 658
5. De Jong JH (2011). A framework for energy saving device (ESD) decision making. International Conference on Ship Efficiency.
6. Karim MM and Naz N (2019). Numerical study on flow around modern ship hulls with rudder-propeller interaction, *J. Mar. Sci. Appl.* Springer, Vol.18, Issue 4, pp. 400 - 416. https://doi.org/10.1007/s11804-019-00113-6
7. Sasaki, N., Kuribayashi, S. and Atlar M (2018). Gate Rudder. The 3rd International Symposium on Naval Architecture and Maritime (INT-NAM). Istanbul, Turkey, pp 89-108.
8. Tacar Z, Sasaki N, Atlar M, Emin K (2020). An investigation into effects of Gate Rudder® system on ship performance as a novel energy-saving and manoeuvring device. *Ocean Engineering,* Vol. 218, Article 108250. https://doi.org/10.1016/j.oceaneng.2020.108250
9. Carchen A, Shi, W, Sasaki N, Atlar M, (2020). Investigation of the manoeuvrability characteristics of a Gate Rudder system using numerical, experimental, and full-scale techniques. *Appl. Ocean Res*., Vol. 106 (3-6), Article 102419. https://doi.org/10.1016/j.apor.2020.102419
10. Fukazawa M, Turkmen S, Marino A, Sasaki N (2018). Full-scale gate rudder performance obtained from voyage data. The 3rd International Meeting -Progress in Propeller Cavitation and its Consequences - Experimental and Computational Methods for Predictions Istanbul, Turkey, pp 71-76.
11. Sasaki N and Atlar M (2019). Scale Effect of Gate Rudder. Sixth International Symposium on Marine Propulsors smp'19, Rome, Italy.
12. Sasaki N, Atlar M, Kuribayashi S (2015). Advantages of twin rudder system with asymmetric wing section aside a propeller: the new hull form with twin rudders utilizing duct effects. *J. Mar. Sci. Technol.* Vol. 21, pp 297–308. https://doi.org/10.1007/s00773-015-0352-z
13. Sasaki N, Kuribayashi S, Fukazawa M, Atlar M (2019). Towards a Realistic Estimation of the Powering Performance of a Ship with a Gate Rudder System. *J. Mar. Sci. Eng*., Vol. 8, pp 43. https://doi.org/10.3390/jmse8010043
14. Sasaki N., Atlar M. (2018). Investigation into the propulsive efficiency characteristics of a ship with the gate rudder propulsion system. In: A. Yücel Odabas¸ı Colloquium Series 3rd International Meeting on Progress in Propeller Cavitation and its Consequences: Experimental and Computational Methods for Predictions. Istanbul, Turkey, pp. 99–107.
15. Turkmen S, Carchen A, Sasaki N, Atlar M (2016) A new energy saving twin rudder system - gate rudder. In: Shipping in Changing Climates Conferences 2015, pp 1-19.
16. The Motorship (2019). New Ducted Propeller Design Offers Fuel Savings; Accessed on 08 Aug 2021. Available at, https://www.motorship.com/news101/
17. Atlar M (2021). Gate Rudder System as a Retrofit for the Next Generation Propulsion and Steering of Ships. Presented at the 2nd Decarburizing Shipping Virtual Forum. Miami, Hamburg.
18. ITTC (2014). Practical Guidelines for Ship Self-Propulsion CFD. Recommended Procedures and Guidelines. 7.5–03–02–01
19. ITTC (2014). Practical Guidelines for RANS Calculation of Nominal Wakes. Recommended Procedures and Guidelines7.5–03–03–02.
20. ITTC (2014). Practical Guidelines for Ship CFD Applications. Recommended Procedures and Guidelines. 7.5–03–02–03
21. ITTC (2014). Practical Guidelines for Ship Resistance CFD. Recommended Procedures and Guidelines. 7.5–03–02–04
22. ITTC (2017). Uncertainty analysis in CFD, verification and validation methodology and procedures. Recommended Procedures and Guidelines. 7.5–03–02–01
23. Siemens (2018). Virtual Tow Tank. Siemens Product Lifecycle Management lnc. CT09301_CM11_4.